Environmental Pollution 279 (2021) 116942

Contents lists available at ScienceDirect

Environmental Pollution

journal homepage: www.elsevier.com/locate/envpol

Molecular mechanisms of zooplanktonic toxicity in the okadaic acid-producing dinoflagellate *Prorocentrum lima*☆

Yufeng Gong [a, b], Keke Zhang [a], Ningbo Geng [c], Minghuo Wu [a], Xianliang Yi [a, *], Renyan Liu [d], Jonathan K. Challis [b], Garry Codling [b, e], Elvis Genbo Xu [f], John P. Giesy [b, g, h, i]

[a] School of Ocean Science and Technology, Dalian University of Technology, Panjin Campus, Panjin, Liaoning, China
[b] Toxicology Centre, University of Saskatchewan, Saskatoon, SK, Canada
[c] CAS Key Laboratory of Separation Sciences for Analytical Chemistry, Dalian Institute of Chemical Physics, Chinese Academy of Sciences, Dalian, China
[d] National Marine Environmental Monitoring Center, Dalian, Liaoning, China
[e] RECETOX Centre, Masaryk University, Kamenice, Brno, Czech Republic
[f] Department of Biology, University of Southern Denmark, Odense, Denmark
[g] Department of Veterinary Biomedical Sciences, University of Saskatchewan, Saskatoon, SK, Canada
[h] Department of Environmental Sciences, Baylor University, Waco, TX, USA
[i] State Key Laboratory of Pollution Control and Resource Reuse, School of the Environment, Nanjing University, Nanjing, People's Republic of China

ARTICLE INFO

Article history:
Received 10 January 2021
Received in revised form
1 March 2021
Accepted 2 March 2021
Available online 12 March 2021

Keywords:
Transcriptomic
Metabolomics
Toxic algal bloom
Zooplankton

ABSTRACT

Prorocentrum lima is a dinoflagellate that forms hazardous blooms and produces okadaic acid (OA), leading to adverse environmental consequences associated with the declines of zooplankton populations. However, little is known about the toxic effects and molecular mechanisms of *P. lima* or OA on zooplankton. Here, their toxic effects were investigated using the brine shrimp *Artemia salina*. Acute exposure of *A. salina* to *P. lima* resulted in lethality at concentrations 100-fold lower than densities observed during blooms. The first comprehensive results from global transcriptomic and metabolomic analyses in *A. salina* showed up-regulated mRNA expression of antioxidant enzymes and reduced non-enzyme antioxidants, indicating general detoxification responses to oxidative stress after exposure to *P. lima*. The significantly up-regulated mRNA expression of proteasome, spliceosome, and ribosome, as well as the increased fatty acid oxidation and oxidative phosphorylation suggested the proteolysis of damaged proteins and induction of energy expenditure. Exposure to OA increased catabolism of chitin, which may further disrupt the molting and reproduction activities of *A. salina*. Our data shed new insights on the molecular responses and toxicity mechanisms of *A. salina* to *P. lima* or OA. The simple zooplankton model integrated with omic methods provides a sensitive assessment approach for studying hazardous algae.

1. Introduction

Diarrhetic shellfish poisoning (DSP), first reported in 1978, is a gastrointestinal illness attributed to consumption of seafood contaminated by DSP such as okadaic acid (OA) and their structural derivatives dinophysistoxins (DTXs) (Yasumoto et al., 1978). These toxins are lipophilic and can accumulate in filter-feeding bivalves, such as mussels, oysters, scallops, or clams, and subsequently enter the marine ecosystems (Lloyd et al., 2013). Exposure to DSP has been frequently reported in various countries, including Japan, South Africa, New Zealand, Australia, Thailand and several European countries (Carvalho et al., 2019; Van Dolah, 2000; Young et al., 2019), representing the primary cause of bans on the harvesting of aquaculture in Japan and Europe (Reguera et al., 2014).

OA, one of the major congeners of DSP, has been identified in numerous species of microalgae in the genera *Dinophysis* (D.) and *Prorocentrum* (P.), including *D. acuminate*, *D. fortii*, *P. lima*, *P. concavum*, *P. rhathymum* and *P. maculosum* (Reguera et al., 2014). Due to the human health concerns associated with OA, most studies have focused on small mammals or *in vitro* mammalian cell lines. Results of those studies have revealed inhibition of serine/threonine protein phosphatases 1 and 2A, apoptosis, cytoskeleton

☆ This paper has been recommended for acceptance by Wen Chen.
* Corresponding author.
E-mail address: yixianliang@dlut.edu.cn (X. Yi).

https://doi.org/10.1016/j.envpol.2021.116942
0269-7491/

disruption, alteration of the cell cycle, and neurotoxicity by exposure to OA (Ferron et al., 2014; Fu et al., 2019; Fujiki and Suganuma, 2009). Deleterious effects of exposure to OA have also been found for embryonic development in fish and frogs (Escoffier et al., 2007; Franchini et al., 2009), and haemocyte function and viability of individuals in clams (*Ruditapes decussatus* and *Anomalocardia brasiliana*), oysters (*Crassostrea gigas*) and mussels (*Perna perna*) (Mello et al., 2010; Prado-Alvarez et al., 2013). Zooplankton can directly accumulate synthetic and natural toxins from the surrounding water and are important for the bio-transfer of DSP up the food chain (Nunes et al., 2006). Murray et al. (2018) reported a 24-h EC_{50} of 1.68 μg/L to *Daphnia pulex*. The copepod *Acartia clausi* could graze on *D. acuminata*, and the ingestion of this toxic dinoflagellated could lead to a lower survival rate (Carlsson et al., 1995). In addition, feeding on toxic diets (i.e., *P. lima*) could negatively affect the reproduction of the other two copepods *A. tonsa* and *Temora longicornis* (Kozlowsky-Suzuki et al., 2009). Overall, there is paucity of available information about the effect of OA on on zooplankton population that is key to maintain the function and structure of aquatic ecosystems.

Artemia salina is a holoplankton species of brine shrimp found in saltwater lakes and tidal estuaries. Due to its ease of culture and multiple life stages, it has been used as a model species for assessing planktonic exposure to harmful compounds (Libralato et al., 2016). *A. salina* has been reported to graze upon several harmful algal blooms, thereby also acting as top-down control (Marcoval et al., 2013). Our recent study has applied *A. salina* to study the toxic effects and toxic mechanisms of *Alexandrum minutum* to zooplanktons. Interestingly, it was found that exposures to alga *A. minutum* and its excreted gonyautoxins caused different effects on *A. salina,* implying the complexity and difference in the toxicity mechanisms of the alga and toxin (Yi et al., 2019). An effective approach to reveal the toxicity mechanisms of environmental pollutants is via the integration of omics techniques (Geng et al., 2019; Liu and Zhu, 2020; Sun et al., 2020). As little is known about the toxic effects and mechanisms of toxic algal blooms, it is important to carry out studies using a broader range of toxic algal species. In this study, toxic effects and molecular mechanisms of *P. lima* and the toxin OA on *A. salina* were investigated by use of a combination of transcriptomics and metabolomics. We hypothesized that exposure to environmentally relevant concentrations of OA or *P. lima* can cause transcriptomic and metabolomics responses of *A. salina* that predict key initial molecular events associated with the toxicity. The aims of this study were to (1) determine the acute toxicity of OA or *P. lima* to *A. salina* of different developmental stages, and to (2) elucidate molecular responses and toxicity mechanisms of *A. salina* to *P. lima* or OA at environmentally relevant concentrations. The results provide a better understanding of adaptive mechanisms of *A. salina* upon exposure to environmentally relevant concentrations of *P. lima* and OA. Moreover, the simple *A. salina* model species combined with sensitive global omic approaches demonstrate good potential and applicable for future algal bloom studies.

2. Materials and methods

2.1. Culture of P. lima and A. salina

The marine dinoflagellate, *P. lima* was originally collected and isolated from Daya Bay, China. To obtain *A. salina* at various life stages, including Instars I, II, III, and adults, commercially available, dehydrated cysts of *A. salina* were incubated for 24 h (h) at 20 ± 1 °C. Instar I larvae (<12 h) were separated based on positive photo-taxis of the larvae. Hatched larvae were maintained for another 24 h, 48 h, and 14 days to obtain instar II and III larvae and adults, respectively. The culture medium for *P. lima* and *A. salina* was made with filtered artificial seawater (FAS) with a salinity of 30 ± 1 ppt.

2.2. Acute toxicity

Twenty-four-hour acute lethality tests were conducted with instar I, II, and III stages or adult *A. salina*. Solvent control (0.1% ethanol in FAS) and seawater control (i.e., FAS) were conducted along with each batch of toxicity tests. There were three replicates with ten individuals per replicate. Larvae or adult *A. salina* were exposed to *P. lima* or OA at a range of doses (25, 50, 100, 200, and 400 μg/L for OA; 1.5, 3, 6, 9, and 18 × 10^3 cells/L for *P. lima*) for 24 h. After exposure, the numbers of dead larvae or adults (completely motionless) were counted under a microscope (Shenying Optical Co., Ltd., Suzhou, China), and the mortality of each treatment was calculated.

2.3. Sublthal exposures for omics analyses

Adult *A. salina* was exposed to 1.5 × 10^3 cells/L of *P. lima* (PL group), 4 μg/L OA (OA_L group), and 20 μg/L OA (OA_H group) for 24 h. Concentrations of 4 μg/L and 20 μg/L were approximately 20% of the LC_{10}, and LC_{10} of OA, respectively. Exposure to FAS served as a control group. There were three replicates per treatment for transcriptomics and four replicates per treatment for metabolomics. Each replicate contained approximately 200 adults that were pooled together as one sample for further omics analyses. Thus, for each treatment, the total numbers of adult *A. salina* used for transcriptomics and metabolomics are 600 and 800, respectively. The exposure strategy was the same as that used for the acute test. After exposure, adult *A. salina* was collected with a mesh net (100 μm pore size) and transferred to 1.5 mL centrifuge tubes. All samples were frozen with liquid nitrogen and stored at −80 °C until further analysis.

2.4. OA and DTXs analysis in exposure solutions

The concentrations of OA and DTXs in exposure solutions from OA_L, OA_H, and PL groups were quantified with high-performance liquid chromatography-tandem mass spectrophotometry (HPLC-MS/MS). See Supplementary information (SI) for details.

2.5. Transcriptomic analysis

Total RNA extraction and cDNA library construction were conducted according to the methods described in our previous study.[17] Due to contamination of RNA in one sample from the control group, a total of 11 sequence libraries were constructed, including 3 replicates in OA and *P. lima* exposure groups and 2 replicates in the control group. The libraries were sequenced on a Hiseq platform (Illumina) by Shanghai Personal Biotechnology Company (Shanghai, China). Processing of raw data and *de novo* assembly were performed by Cutadapt (version 1.15) and Trinity software (r20140717, K-mer 25 bp). Assembled unigenes were annotated for function against several public databases, including the NCBI non-redundant protein sequences (NR) database, Gene Ontology (GO) database, Kyoto Encyclopedia of Genes and Genome (KEGG) database, evolutionary genealogy of genes: Non-supervised Orthologous Groups (eggNOG) database and Swiss-Prot database with a threshold E-value ≤ $1e^{-5}$ (Conesa et al., 2005). Clean reads were mapped to each assembled unigene by RSEM software (Li and Dewey, 2011). Transcript abundances were measured as fragments per kilobase of transcript sequence per millions base pairs sequenced (FPKM). The transcriptomics data was validated and

compared with the results from quantitative real-time PCR (qRT-PCR). Eight unigenes were randomly selected and housekeeping glyceraldehyde-3-phosphate dehydrogenase (GAPDH) was employed as the reference gene. See more details in SI 2.

2.6. Metabolomics analysis

Metabolites were extracted with a mixture of methanol/water (4:1, v:v) according to a previously published method (Wang et al., 2018). A pseudo-targeted metabolomics strategy was performed for global analysis of the *A. salina* metabolome (Zheng et al., 2020). Details of the preparation of samples and instrumental analysis are given in SI 3. Metabolites were annotated by MS/MS matching to experimental spectra in the Human Metabolome Database (HMDB) and the METLIN database. Commercially available standards were further used to validate these annotations. For quantification, peak areas of each metabolite were normalized to corresponding internal standards after peak alignment and missing value interpolation. A quality control (QC) sample was prepared by pooling 10 μL of aliquots from each sample. QC samples were analyzed before analysis of real biological samples for system equilibration and inserted after every 6 samples to monitor system stability. Procedural blank samples (i.e., extraction without actual sample) were also prepared and analyzed to filter any contaminations that were introduced during sample preparation.

2.7. Statistics

For transcriptomics data, differentially expressed genes (DEGs) were filtered by DESeq (version 1.18.0) with the criteria of P-value < 0.05 and fold change (FC) > 2. DEGs were further applied to GO and KEGG pathway enrichment analyses and false discovery rate (FDR) < 0.05 were adopted as the threshold for significant enrichment. For metabolomics data, all data were log-transformed to achieve normally distributed data before statistical analysis. Differential metabolites (DMs) were determined by one-way ANOVA followed by Fisher's LSD test. FDR <0.05 was considered as significant. Statistical analyses were conducted by use of R (version 3.6.2). The t-distributed stochastic neighbor embedding (tSNE) scatterplot was generated after Z-score scaling of the transcriptomics data by use of the Rtsne package. Upset plot, partial least squares-discriminant analysis (PLS-DA), and hierarchical clustering analysis were produced by UpsetR, Ropls, and Pheatmap packages, respectively. A transcriptional effect level index (TELI) for each exposure group was calculated according to Gou and Gu (2011). Chemical similarity enrichment analysis (ChemRICH) was performed on the annotated metabolomics dataset (Barupal and Fiehn, 2017). Chemical clusters with FDR<0.05 were considered significant. Cluster direction is the median $\log_2$ fold change relative to the control of DMs in each metabolite cluster (Contrepois et al., 2020).

3. Results and discussion

3.1. Acute toxicity

LC_{50} values of OA were 170.0 (95% CI: 143.4–201.7), 133.8 (111.0–161.4), 152.4 (122.5–189.6) and 186.4 (156.1–222.6) μg/L to *A. salina* at Instar I, Instar II, Instar III, and adult stage, respectively (Fig. 1a). As revealed by their overlapping 95% CI of LC_{50} values, the toxic potencies of OA were not significantly different for *A. salina* among developmental stages. To date, available data on acute lethality of OA to aquatic organisms is still scarce. Previous studies showed that 96h LC_{50} of OA to larvae of black sea bream *Sparus microcephalus* was 20.7 μg/L, but the hatching of the fish embryos

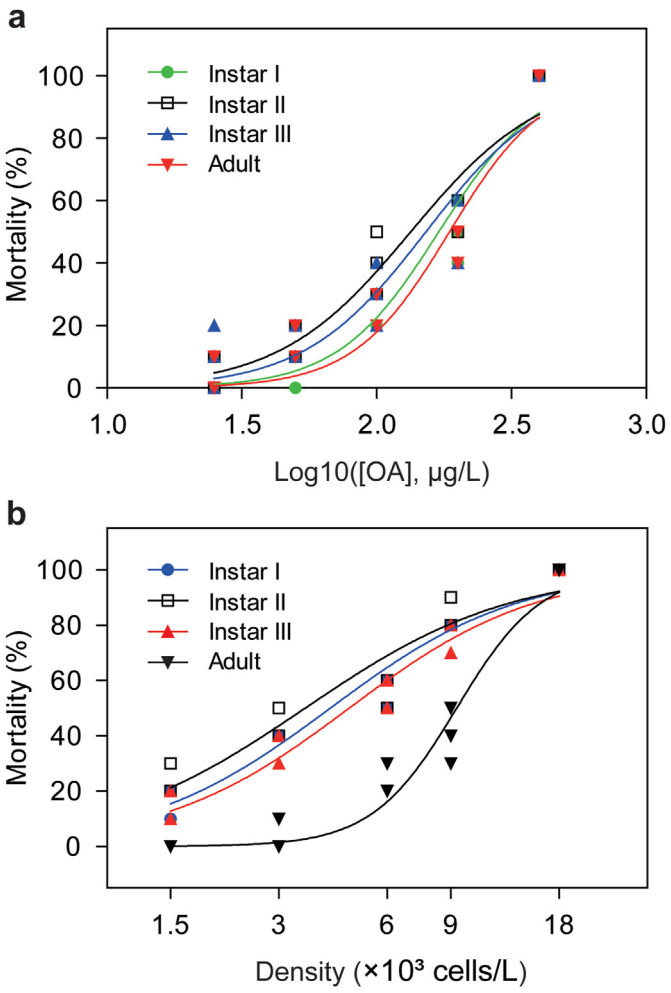

Fig. 1. Acute toxicity of OA **(a)** or *P. lima* **(b)** to *A. salina* at different developmental stages. Four developmental stages (Instar I, II, III, and adult) were exposed for 24-h toxicity test. There were three replicates with ten individuals per replicate for each exposure.

was not affected, which indicated that embryos of fish were relatively tolerant to exposure to OA (Jiang, 2011). Toxicity of OA has also been observed in medaka fish embryos (*Oryzias latipes*) with an LC_{50} of 520 μg/L (Escoffier et al., 2007). Our results show that *A. salina* is more sensitive to OA exposure than medaka fish embryos. The OA levels in seawater were at 3.6 ng/L and between 1.4 and 89.5 ng/L in seawater samples collected in Flødevigen (Norway) and Qingdao (China), respectively (Li et al., 2014; Torgersen et al., 2008). These concentrations are lower than those used in this study, indicating that OA is unlikely to pose acute toxicity at realistic environmental concentrations.

The sensitivity of *A. salina* to exposure to *P. lima* was not significantly different among different larval stages, with 24 h LC_{50} values of 4.17 (95%CI: 3.68–4.73), 3.55 (95%CI: 2.95–4.23) and 4.10 (95%CI: 4.08–5.42) $\times$ 10^3 *P. Lima* cells/L for Instar I, Instar II and Instar III, respectively (Fig. 1b). Unlike OA, adult *A. salina* was less sensitive to *P. lima*, with an LC_{50} of 9.35 $\times$ 10^3 (95%CI: 8.45–10.29) cells/L. At the same exposure density of *P. lima* (strain PL2V), no mortality of juvenile sea bass (*Dicentrarchus labrax*) was observed, although juvenile fish behaved abnormally with fast left-right turns, surface swims, and jumps (Ajuzie, 2008), which suggested that *P. lima* is more lethal to planktonic *A. salina* than juvenile sea bass. It is worth noting that these LC_{50} values of *P. lima* to *A. salina*

are orders of magnitude lower than the levels reported during red tides (e.g., 5.0×10^6 cells/L) (Li et al., 2011). The observed acute toxicity reported here implies a decline of *A. salina* populations exposed to these blooms. Grazing of *P. lima* by *A. salina* has been observed and some cases reported mortality of artemia after ingestion of only one cell of *P. lima* (Ajuzie, 2007), which confirms the acute toxicity of *P. lima* to *A. salina*.

3.2. Transcriptome assembling and annotation

A total of 570,791 transcripts were obtained, which were clustered into 474,366 unigenes (Table S3). The percentages of Q30 and GC content were 93.26–95.23% and 40.22–41.11%, respectively. According to functional gene annotation analysis with an *E*-value cutoff of $<10^{-5}$, the transcripts were successfully annotated by five public databases, namely NR (10.16%), GO (26.73%), KEGG (0.99%), eggNOG (11.88%), and Swissprot (7.94%) (Table S4). Matches with an *E*-value of 10^{-15} to 10^{-5} had the largest ratio and 14.06% of unigenes had a similarity greater than 80% to available animal sequences (Figure S1a and b). 5.26% of *A. salina* unigenes matched that from *Daphnia magna*, followed by *D. pulex* (4.55%) (Figure S1c). Moreover, annotated unigenes assigned to KEGG pathways were mainly associated with metabolism, genetic information processing, environmental information processing, cellular processes, and organismal systems (Figure S2). Enriched GO terms with annotated transcripts were also shown in Figure S3. Although *A. salina* has been widely employed in ecotoxicology (Gutner-Hoch et al., 2019; Lu et al., 2018; Zhu et al., 2017), genomic sequencing of this ecologically important species has not been conducted and only few reports on its transcriptome are available (De Vos et al., 2019; Yi et al., 2019). The transcriptomic data reported here provide valuable molecular resources for understanding the responses of *A. salina* under stress. The raw data were deposited at NCBI SRA (accession number PRJNA657177).

3.3. Global omic responses

The t-SNE plot (Fig. 2a) showed that samples from exposure groups were distinct from each other, demonstrating the altered transcriptional profiles after exposure to OA or *P. lima*. Transcriptional effect level index (TELI) values (Gou et al., 2011), which consider both number of DEGs and the magnitude of altered gene expression to exposure, represent an integrated endpoint index for the overall transcriptomics changes in *A. salina*. TELI values in all exposure groups were higher than that of the control group, supporting that OA or *P. lima* exposure induced significant alterations in *A. salina* transcriptome (Fig. 2b). Relative to control, a total of 1233, 2573, and 1024 transcripts were identified as DEGs in OA_L, OA_H, and PL groups, respectively. Most of the DEGs were up-regulated, accounting for 69.2, 64, and 95.7% of total DEGs in each exposure group (Fig. 2c). Although OA_L and OA_H shared a large number of DEGs (823 DEGs), only 32 transcripts were communally altered among all exposure groups (Figure S4a). This result suggested that exposure to either OA or *P. lima* resulted in distinct transcriptional responses. The OA_H group exhibited more DEGs than the PL group but exhibited a lower value of TELI. This might be attributed to the greater average fold change of DEGs induced by PL exposure (Figure S5). These results demonstrated that exposure to 1.5×10^3 *P. lima* cells/L caused greater alterations in the transcriptome of *A. salina* and revealed the potential benefits of using TELI to evaluate overall alterations in transcriptomics. DEGs were further subjected to KEGG (Fig. 2d) and GO (Figure S6, S7, and S8) enrichment analysis. Fourteen KEGG pathways were significantly enriched in OA or *P. lima* exposure groups, and most of them were up-regulated (Fig. 2d and Table S7). These significantly enriched KEGG pathways were mainly involved in processing genetic information and metabolism. In addition, eight DEGs were randomly selected for technical validation of transcriptomics data. These genes include proteasome subunit beta type-2, phosphoserine aminotransferase 1, serine-pyruvate aminotransferase, cytochrome *c* oxidase subunit 1, trypsin-1, phosphoglycerate kinase, aspartate aminotransferase (cytoplasmic), and tyrosine aminotransferase (Table S2). These genes mainly regulate proteolysis, oxidative phosphorylation, and amino acid transamination, which could indicate the cellular processes altered by exposure to *P. lima* and OA. As shown in Figure S9, the gene expression levels of these

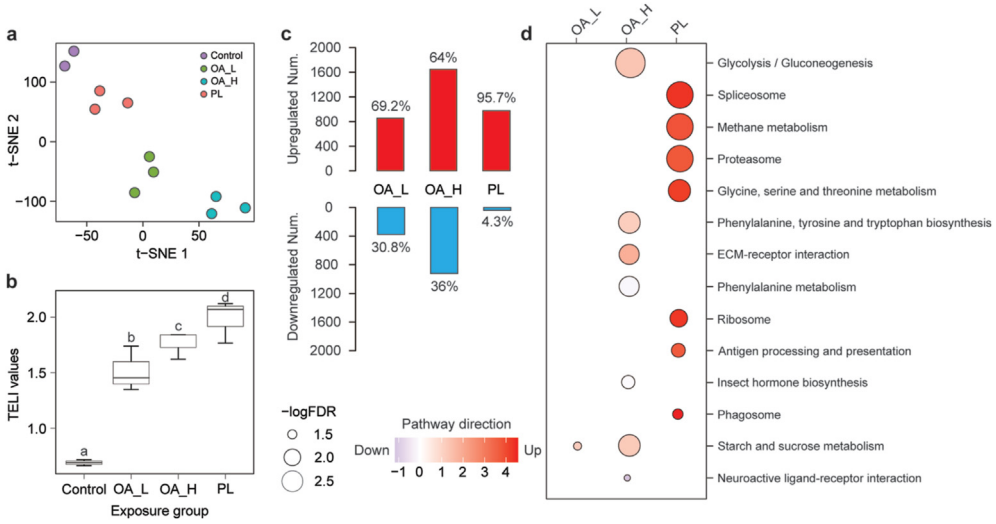

Fig. 2. Changes in the transcriptional profile of adult *A. salina* after exposure to OA or *P. lima* cells. (a) t-SNE clustering of *A. salina* transcriptome. Data were log-transformed and scaled to the Z-score. (b) TELI values of transcription fingerprint in the control and treated groups. (c) Numbers of up-regulated and down-regulated DEGs in each exposure group. Values on top of each bar indicate the percentage of up-regulated or down-regulated DEGs. (d) KEGG enrichment of DEGs. OA_L: 4 μg/L of OA exposure group; OA_H: 20 μg/L of OA exposure group; PL: 1.5×10^3 cell/L of *P. lima* exposure group. Pathway direction is the median $\log_2$ fold change of DEGs relative to control in each pathway (blue, downregulated; red, upregulated). *P* values were corrected for multiple hypotheses by Benjamini-Hochberg method and KEGG pathways with FDR <0.05 were treated as significant. The dot size represents pathway significance. (For interpretation of the references to color in this figure legend, the reader is referred to the Web version of this article.)

eight representative genes measured by qRT-PCR analysis were consistent with that from RNA-seq, which independently verified our transcriptomics data.

The pseudo-targeted metabolomics analysis revealed substantial changes in metabolism in adult *A. salina* exposed to OA or *P. lima* treatment (Fig. 3). A total of 462 metabolites were measured. The PLS-DA analysis was conducted for all detected metabolites and the QC samples were found tightly clustered (Fig. 3a). Additionally, 96.5% of detected metabolites showed relative standard deviation (RSD) less than 20% (Figure S10). These results demonstrated good reproducibility of the method applied for metabolomics. In the PLS-DA score plot, samples from treated groups were all separated from the control group. This suggested that exposure to both *P. lima* and OA disturbed normal metabolic processes of *A. salina*. A total of 233 metabolites were identified as DMs. Among them, 69 DMs were annotated by use of their MS^2 spectra (Fig. 3c and Table S5), and some of them were confirmed by commercial standards during the method development stage. Compared to the control group, relative abundances of 8, 28, and 77 metabolites were significantly greater, while 21, 7, and 135 metabolites were significantly less in the OA_L, OA_H, and PL group, respectively (Fig. 3b). Only 4 metabolites were altered in all exposure groups (Figure S4b). Together these results suggested differential metabolomics responses of *A. salina* to OA or *P. lima* exposure. Annotated metabolites were further subjected to ChemRICH analysis based on chemical similarity and ontology mapping. Unlike canonical pathway enrichment, e.g., KEGG pathway enrichment, ChemRICH enables study-specific and background-independent enrichment analysis.[26, 27] The ChemRICH analysis showed a marked decrease of carnitine, lysophosphatidylcholines (LPC), amino acids, unsaturated phosphatidylcholines (PC) and sphingomyelins (SM) in *A. salina* from PL group (Fig. 3d) in comparison to control. Unsaturated and saturated fatty acids were also significantly increased in the PL group. Moreover, differential regulation of carnitine, pyrimidine nucleosides, and SM were observed in OA exposure groups.

3.4. OA and DTXs measurements

The actual exposure concentrations of OA and DTXs in each group were measured with LC-MS/MS (Table S6). The concentrations of OA in OA_L and OA_H treatment groups were 5.10 ± 1.56 μg/L and 20.85 ± 0.40 respectively. In *P. lima* exposure solutions, OA and DTX1 were detected at concentrations of 9.83 ± 1.56 and 5.47 ± 0.49 μg/L respectively but neither DTX2 nor YTX were detected. Based on equivalency factors defined by European Food Safety Authority (EFSA, 2008), the OA equivalent (OAeq) of *P. lima* exposure group was 15.30 ± 2.06 μg/L, which was lower than that of OA_H group. However, *P. lima* caused more significant effects on transcriptomics and metabolomics profiles of *A. salina* than did OA alone. This result implied that the OA and DTXs secreted by *P. lima* were not the only contributors to *P. lima* toxicity. Although OA and DTX1 were thought to be the major toxins produced by P. lima for many years (Lee et al., 1989), recent studies showed that *P. lima* could excrete other toxins such as esterified derivatives of OA and DTX1 (Wu et al., 2020) which might have contributed to toxic potency of *P. lima*. In addition, *A. salina* is a

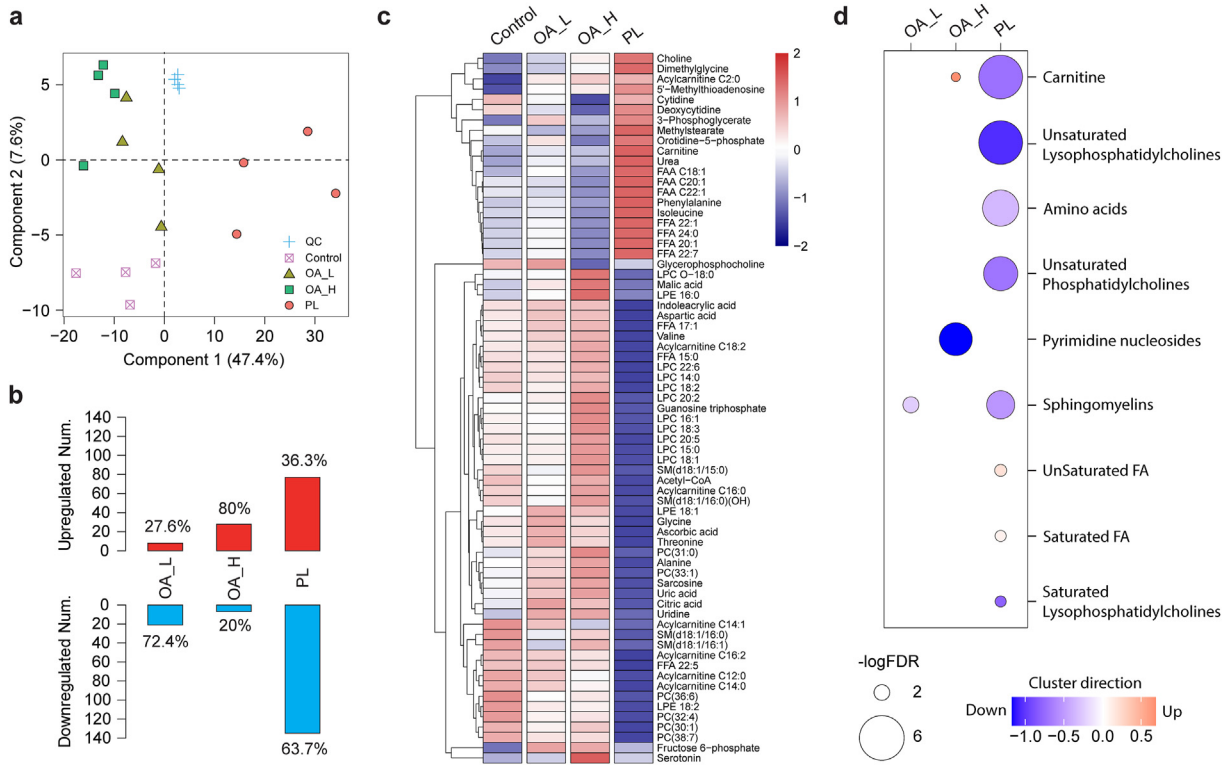

Fig. 3. Changes in metabolome of adult *A. salina* after exposure to OA or *P. lima*. (a) PLS-DA score plot of *A. salina*. $R^2 = 0.84$; $Q2 = 0.76$. (b) The number of significantly up-regulated and down-regulated differential metabolites (DMs) in each exposure group. The values on top of each bar indicate the percentage of up-regulated or down-regulated DMs. (c) Hierarchical clustering analysis of DMs. Data were log-transformed and Z-score scaled. FFA: free fatty acid; FAA: fatty acid amide; LPC O: ether-linked lysophosphatidylcholine; LPC: lysophosphatidylcholine; LPE: lysophosphatidylethanolamine; PC: Phosphatidylcholine; SM: sphingomyelin. (d) Significantly enriched metabolite clusters by ChemRICH analysis. OA_L: 4 μg/L of OA exposure group; OA_H: 20 μg/L of OA exposure group; PL: 1.5×10^3 cell/L of *P. lima* exposure group. Pathway direction is the median $\log_2$ fold change of DMs relative to control in each cluster (blue, downregulated; red, upregulated). *P* values were corrected for multiple hypotheses by Benjamini-Hochberg method and metabolites clusters with FDR <0.05 were treated as significant. The dot size represents significance. (For interpretation of the references to color in this figure legend, the reader is referred to the Web version of this article.)

continuous non-selective filter-feeder (Landau et al., 1985). Direct ingestion of *P. lima* cells by *A. salina* has been reported (Ajuzie, 2007), and thereby the intra-cellular toxins produced by *P. lima* might also enhance its toxicity to *A. salina*. *A. salina* can grow to about 10–12 mm in body length (Domenech, 1980). In contrast, *P. lima* varies from 31 to 57 μm in length and 20–46 μm wide. *A. salina* collects suspended food particles with the fine filtratory setae on the trunk limbs as they swim (Savage and Knott, 1998; Riisgård et al., 2015). However, the gills of *A. salina* are on the outer side of the limb bases and have no carapace. Without the protection of carapace, the gills of *A. salina* could be much more susceptible. Thus, direct contact of gills of *A. salina* to P. lima cells could provide another possible explanation for greater toxicity of P. lima than its secreted toxins. Yan et al. (2007) compared toxic potencies of various algal species, including Prorocentrum donghaiense, Karenia mikimotoi, and A. catenella to two crustacean species, Neomysis awatschensis and *A. salina*. The authors proposed that direct contact between gills of *A. salina*, might have led to higher toxicity of these algal species to *A. salina* than to K. mikinotoi the gills of which are covered by a carapace.

3.5. Toxicity mechanisms

In the present study, we found distinct trancriptomics and metabolomics profiles in *A. salina* after exposure to *P. lima* or OA at environmentally relevant concentrations. By integrating transcriptomics and metabolomics data that could reveal biological pathways affected, we proposed four possible mechanisms for *P. lima* toxicity: (1) induction of oxidative stress, (2) protein damage, (3) disruption of energy metabolism, and (4) membrane damage. As for exposure to OA, the major effects were oxidative stress and induction of chitin catabolic metabolism.

3.5.1. Oxidative stress

A variety of antioxidation/detoxification genes can be activated in aquatic organisms in response to chemical stressors. These include genes encoding glutathione *S*-transferase (*Gst*), glutathione *S*-transferase Pi 1 (*Gstp1*), catalase (*Cat*), catalase-peroxidase (*KatG*), aldehyde dehydrogenase (*Aldh*), and cytochrome P450 4 monooxygenases (*Cyp4*) (Guo and Ki, 2013; Lauritano et al., 2013; Lavarías et al., 2011; Liu et al., 2019; Singh et al., 2013; Snyder, 2000). Expression changes of these genes are early biomarkers for chemical-induced oxidative stress. In this study, significantly upregulated expressions of *Gstp1*, *Cat1*, *KatG*, and *Aldh8a1* were observed in the PL group (Fig. 4a), which suggested oxidative stress caused by exposure to *P. lima*. Also, two non-enzymatic antioxidants, ascorbic and uric acids, were significantly down-regulated in the PL group (Fig. 4b). Ascorbic acid and uric acid are potent water-soluble antioxidants and protect cells by interacting with reactive oxygen species (ROS) (Bendich et al., 1986; Parvez and Raisuddin 2006). The reduced abundance of ascorbic and uric acids could result from increased utilization for scavenging ROS. Similarly, the upregulated expression of the *Gst* gene was also seen in groups exposed to OA. *Gst* catalyzes the conjugation of the tripeptide glutathione (GSH) to xenobiotic substrates which makes those compounds more hydrophilic for the purpose of detoxification (Oakley et al., 2011). Thus, the lipophilic OA could be one of the factors that contributes to inductions of *Gst* expression in *A. salina* after exposure to *P. lima* or OA. Meanwhile, exposure to OA significantly up-regulated the expression of *Cyp4c3* gene that is involved in the clearance of xenobiotics by oxidative modifications (Lee et al., 1989). These results demonstrated that oxidative stress was caused by exposure to either *P. lima* or OA as well as activation of detoxification mechanisms in *A. salina*. This is in line with previous studies that also reported greater oxidative stress in other aquatic organisms exposed to OA or *P. lima* (Dou et al., 2020; Huang et al., 2015; Prego-Faraldo et al., 2017; Souid et al., 2018).

3.5.2. Protein damage

Exposure to ROS can destabilize and inactivate proteins (Ezraty

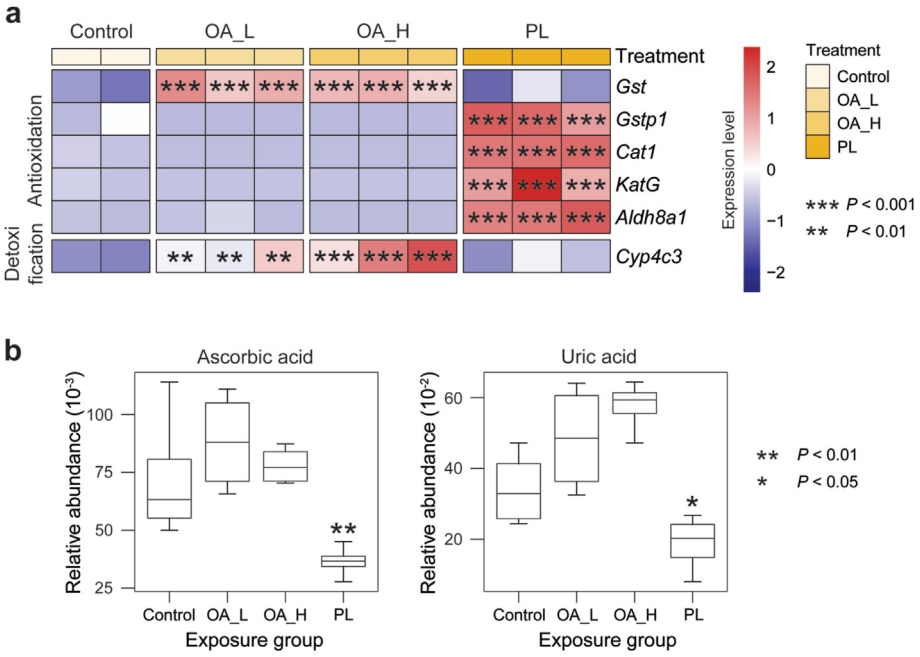

Fig. 4. Antioxidation/detoxification genes (a) and antioxidative metabolites (b) annotated in adult *A. salina* in response to OA or *P. lima* exposure. OA_L: 4 μg/L of OA exposure group; OA_H: 20 μg/L of OA exposure group; PL: 1.5 × 10^3 cell/L of *P. lima* exposure group. *Gst*: glutathione S-transferase; *Gstp1*: glutathione S-transferase P1; *Cat1*: catalase isozyme 1; *KatG*: catalase-peroxidase; *Aldh8a1*: aldehyde dehydrogenase family 8 member A1; *Cyp4c3*: cytochrome P450 4c3. Data were Z-scaled for heat map plot. ***, *P* value < 0.001; **, *P* value < 0.01; *, *P* value < 0.05.

et al., 2017). Heat shock proteins (HSP) are generally related to the maintenance of cellular protein integrity and protect cells from environmental stress, especially for heat and oxidative stress (Feder and Hofman, 1999). Specifically, *Hsp70* helps prevent protein aggregation and promote protein transport for degradation (Leu et al., 2009). *Hsp60* is implicated in the stabilization of non-native proteins and unfolding misfolded proteins generated under stress for proteolysis (Saibil, 2013). In the present study, significantly up-regulated expressions of *Hsp60* and *Hsp70* were observed in the PL exposure group, implying that oxidative stress induced by *P. lima* might contribute to protein damage. *P. lima* exposure also resulted in up-regulation of mRNA expression of several proteasome subunits. Proteasomes are proteolytic complexes that can degrade damaged proteins by proteolysis (Bochtler et al., 1999). These data suggested an enhanced proteasomal clearance of damaged proteins in *A. salina* after *P. lima* exposure. We also found significantly increased mRNA levels of genes encoding ribosome and spliceosome. Overexpression of these genes indicated an up-regulated mRNA splicing, ribosomal assembly, and consequently protein synthesis, which can protect *A. salina* from ROS induced protein damage. Similarly, Asselman et al. (2012) reported differential regulation of the ribosome in *D. pulex* in response to *Microcystis aeruginosa* exposure. Significantly disrupted metabolism of amino acid (Figure S11a) and increased gene expression of aminotransferases, including phosphoserine aminotransferase, serine-pyruvate aminotransferase, and alanine-glyoxylate aminotransferase 2 were also found in *A. salina* after exposure to *P. lima* (Figure S11b), which suggested an activated transamination. The significantly altered exporessions of these aminotransferases by *P. lima* were also independently verified by qRT-PCR (Figure S9). Taken together, these findings suggest that proteasomal clearance of damaged proteins and ribosomal protein synthesis were activated in adult *A. salina* to cope with the *P. lima* exposures (Fig. 5a).

3.5.3. Disruption of energy metabolism

Another identified pathway significantly affected by exposure to *P. lima* is energy metabolism (Fig. 5b). This effect was first suggested by the up-regulated fatty acid oxidation, which was based on the increased expression of long chain acyl-CoA synthetases (*Lacs*) and peroxisomal acyl-coenzyme A oxidase 3 and decreased acylcarnitines levels. Additional evidence was the induction of genes involved in the oxidative phosphorylation pathway, including succinate dehydrogenase flavoprotein subunit (*Sdha1*), V-type proton ATPase subunit E1 (*Vha-e1*), and V-type proton ATPase subunit B (*Vha-b1*). Increased fatty acid oxidation, in combination with the up-regulated oxidative phosphorylation, suggested an enhanced energy production and conversion in *A. salina* after *P. lima* exposure. The enhanced energy production may be a compensatory mechanism to banlance the increased ATP demand and can facilitate homeostasis under the stress induced by *P. lima* exposure (Sokolova et al., 2012). The increased energy output can support ribosomal protein synthesis or stabilize misfolded proteins. Differential regulation of energy metabolism has been observed in aquatic crustaceans after exposure to environmental pollutants (Li et al., 2017; Song et al., 2016). For instance, Lin et al. (2016) reported that exposure to ZnO NPs, bulk ZnO, or $ZnSO_4 \cdot 7H_2O$ significantly up-regulated several enzymes of energy synthesis in *D. pulex*, including glyceraldehyde-3-phosphate dehydrogenase, mitochondrial malate dehydrogenase, and ATP synthase. The increased energy metabolism observed here could be considered as one of the major mechanisms of adult *A. salina* to cope with adverse effects induced by exposure to *P. lima* cells.

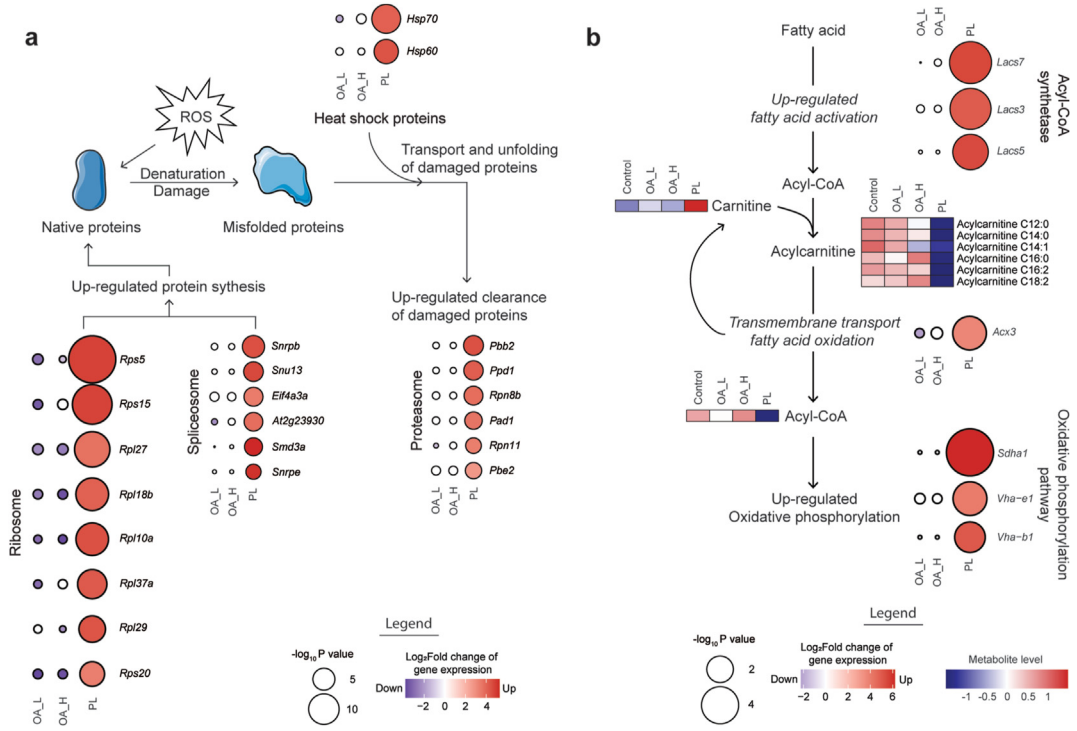

Fig. 5. The major mechanisms in adult *A. salina* to cope with exposure to *P. lima*. (a) Enhanced proteasomal clearance of damaged proteins and ribosomal protein synthesis; (b) Up-regulated energy metabolism. Alterations in gene expression level were presented by bubble blot. The color of the bubble represents the $\log_2$ fold change of DEGs relative to control (blue, downregulated; red, upregulated). The bubble size indicates the $-\log_{10}$ *P*-value. The metabolite profiles were presented by heat map plot. OA_L: 4 μg/L of OA exposure group; OA_H: 20 μg/L of OA exposure group; PL: 1.5×10^3 cell/L of *P. lima* exposure group. The annotation of genes is provided in Table S9. (For interpretation of the references to color in this figure legend, the reader is referred to the Web version of this article.)

3.5.4. Membrane damage

Choline-containing phospholipids including LPC, PC, SM, and glycerophosphocholine (GPC) are major constitutes of the eukaryotic membrane. For example, PC represents about 40% of phospholipids in most cellular membranes (Klein 2000). SM can form "lipid raft" microdomains with cholesterol and proteins on plasma membranes, which have key regulatory functions in protein trafficking and signal transductions (Ando et al., 2015; Bieberich, 2018). In this study, LPC, PC, SM, and GPC levels were all significantly decreased while the choline level was significantly increased in PL group compared to the control (Figure S12). This indicated an up-regulated degradation of choline-containing phospholipids and the release of choline. Breakdown of choline-containing phospholipids could be an indicator of membrane damage caused by exposure to *P. lima*.

3.5.5. Dysregulation of chitin metabolism

Disruption of chintin metabolism in crustaceans has been reported to be caused by exposure to various environmental stresses, including heavy metals (Poynton et al., 2007; Connon et al., 2008), nonomaterials (Lin et al., 2020; Liu et al., 2020), and organic contaminants (Hook et al., 2014). According to results of the GO enrichment analysis, most of the enriched terms in OA exposure groups were related to chitin catabolic metabolism, for example, chitin catabolic process, glucosamine-containing compound catabolic process, aminoglycan catabolic process, amino sugar catabolic process, structural constitute of the cuticle, and chitinase activity (Figure S6 and S7). The crustacean exoskeleton is composed of cuticle proteins and chitin (Charles, 2010). The molting process requires coordinated regulation of chitin metabolism and cuticle protein synthesis (Merzendorfer and Zimoch, 2003; Rocha et al., 2012). In this study, the up-regulated catabolism of chitin implied potential adverse effects of OA exposure on molting process or sheath morphogenesis in *A. salina*. Disrupted molting process has been demonstrated to be directly related to reproduction of crustaceans, thus increased chitin catabolic metabolism by exposure to OA might ultimately affect reproduction of *A. salina* (Poynton et al., 2008). Moreover, the exoskeleton helps to maintain body structure in aquatic crustaceans and can contribute to resist environmental stressors. Therefore, the up-regulated chitin catabolism further suggested the potentially decreased resistibility to environmental stressors and reduced fitness of *A. salina* after exposure to OA.

3.6. Environmental implications

The current study presented the first comprehensive molecular data on the toxicity and mechanisms in a model zooplankton *A. salina* after environmentally realistic exposures to a common harmful algae *P. lima* and OA. First, *P. lima* was found to cause lethality of *A. salina* at concentrations that are orders of magnitude lower than those reported to occur during blooms of hazardous algae (5.0×10^6 cells/L) (Li et al., 2011). The sublethal exposure to environmentally relevant concentrations of *P. lima.* (1.5×10^3 cells/L) resulted in significant transcriptomic and metabolomic alterations of adult *A. salina*, involving oxidative stress defense, clearance of damaged protein, energy metabolism, and membrane disruption. These effects were observed at *P. lima* concentrations comparable to those found in coastal marine environments (up to 1.52×10^3 cells/L) (Gharbia et al., 2012), and much lower than those reported when toxic blooms of algae have occurred (5.0×10^6 cells/L) (Li et al., 2011), demonstrating the sensitivity of *A. salina* to exposure of *P. lima* and suggesting the likely adverse impacts in the real environment. The wide ecological distribution, the ease of culturing *A. salina,* and relatively fast development time make it ideal for the fast development of a comprehensive toxicological system coupled with state of the art transcriptomic and metabolomic endpoints. The high sensitivity of *A. salina* to toxic alga species advance it as the model organism to investigate the adverse impacts of harmful algal blooms. Future research comparing the different responses of other holoplanktonic organisms to more harmful alga species and toxins is suggested to provide a holistic understanding of the ecological consequences of harmful alga bloom.

Declaration of competing interest

The authors declare that they have no known competing financial interests or personal relationships that could have appeared to influence the work reported in this paper.

Acknowledgements

This work was financially supported by National Science Foundation of China with the Grants No. 41606131 and No. 41576120. The authors were also supported by the State Environmental Protection Key Laboratory of Coastal Ecosystem (Grant No. 201812), Dalian University of Technology via the Fundamental Research Funds for the Central Universities (DUT17RC(4)37), and in part by the Canada First Research Excellence Fund (#419205) and Fisheries and Oceans Canada's National Contaminants Advisory Group. Prof. Giesy was supported by the Canada Research Chairs Program of the Natural Sciences and Engineering Research Council of Canada (NSERC). Dr. Codling was supported by the H2020-MSCA-IF-2018 fellowship (839243), CETOCOEN PLUS project of the ESIF (CZ.02.1.01/0.0/0.0/15_003/0000469), and the RECETOX research infrastructure (LM2018121). Dr. Challis was supported by Banting post-doctoral fellowship. Dr. Xu acknowledges the support of Department of Biology, University of Southern Denmark.

Appendix A. Supplementary data

Supplementary data to this article can be found online at https://doi.org/10.1016/j.envpol.2021.116942.

References

Ando, J., Kinoshita, M., Cui, J., Yamakoshi, H., Dodo, K., Fujita, K., Murata, M., Sodeoka, M., 2015. Sphingomyelin distribution in lipid rafts of artificial monolayer membranes visualized by Raman microscopy. Proc. Natl. Acad. Sci. Unit. States Am. 112, 4558. https://doi.org/10.1073/pnas.1418088112.

Ajuzie, C.C., 2007. Palatability and fatality of the dinoflagellate *Prorocentrum lima* to *Artemia salina*. J. Appl. Phycol. 19, 513–519. https://doi.org/10.1007/s10811-007-9164-9, 2007.

Ajuzie, C.C., 2008. Toxic *Prorocentrum lima* induces abnormal behaviour in juvenile sea bass. J. Appl. Phycol. 20, 19–27. https://doi.org/10.1007/s10811-007-9176-5.

Asselman, J., De Coninck, D.I.M., Glaholt, S., Colbourne, J.K., Janssen, C.R., Shaw, J.R., De Schamphelaere, K.A.C., 2012. Identification of pathways, gene networks, and paralogous gene families in *Daphnia pulex* responding to exposure to the toxic cyanobacterium *Microcystis aeruginosa*. Environ. Sci. Technol. 46, 8448–8457. https://doi.org/10.1021/es301100j.

Barupal, D.K., Fiehn, O., 2017. Chemical similarity enrichment analysis (ChemRICH) as alternative to biochemical pathway mapping for metabolomic datasets. Sci. Rep. 7, 14567. https://doi.org/10.1038/s41598-017-15231-w.

Bendich, A., Machlin, L.J., Scandurra, O., Burton, G.W., Wayner, D.D.M., 1986. The antioxidant role of vitamin C. Adv. Free Radic. Biol. Med. 2, 419–444. https://doi.org/10.1016/S8755-9668(86)80021-7.

Bieberich, E., 2018. Sphingolipids and lipid rafts: novel concepts and methods of analysis. Chem. Phys. Lipids 216, 114–131. https://doi.org/10.1016/j.chemphyslip.2018.08.003.

Bochtler, M., Ditzel, L., Groll, M., Hartmann, C., Huber, R., 1999. The proteasome. Annu. Rev. Biophys. Biomol. Struct. 28, 295–317. https://doi.org/10.1146/annurev.biophys.28.1.295.

Carvalho, I.L.D., Pelerito, A., Ribeiro, I., Cordeiro, R., Núncio, M.S., Vale, P., 2019. Paralytic shellfish poisoning due to ingestion of contaminated mussels: a 2018 case report in Caparica (Portugal). Toxicon 4, 100017. https://doi.org/10.1016/j.toxcx.2019.100017.

Carlsson, P., Granéli, E., Finenko, G., Maestrini, S.Y., 1995. Copepod grazing on a

phytoplankton community containing the toxic dinoflagellate *Dinophysis acuminata*. Jounal of Plankton Research 17, 1925–1938. https://doi.org/10.1093/plankt/17.10.1925.
Charles, J.P., 2010. The regulation of expression of insect cuticle protein genes. Insect Biochem. Mol. Biol. 40, 205–213. https://doi.org/10.1016/j.ibmb.2009.12.005.
Conesa, A., Götz, S., García-Gómez, J.M., Terol, J., Talón, M., Robles, M., 2005. Blast2GO: a universal tool for annotation, visualization and analysis in functional genomics research. Bioinformatics 21, 3674–3676. https://doi.org/10.1093/bioinformatics/bti610.
Connon, R., Hooper, H.L., Sibly, R.M., Lim, F.-L., Heckmann, L.-H., Moore, D.J., Watanabe, H., Soetaert, A., Cook, K., Maund, S.J., Hutchinson, T.H., Moggs, J., Coen, W.D., Iguchi, T., Callaghan, A., 2008. Linking molecular and population stress responses in *Daphnia magna* exposed to cadmium. Environ. Sci. Technol. 42, 2181–2188. https://doi.org/10.1021/es702469b.
Contrepois, K., Wu, S., Moneghetti, K.J., Hornburg, D., Ahadi, S., Tsai, M.S., Metwally, A.A., Wei, E., Lee-McMullen, B., Quijada, J.V., Chen, S., Christle, J.W., Ellenberger, M., Balliu, B., Taylor, S., Durrant, M., Knowles, D.A., Choudhry, H., Ashland, M., Bahmani, A., Enslen, B., Amsallem, M., Kobayashi, Y., Avina, M., Perelman, D., Rose, S.M.S.F., Zhou, W., Ashley, E.A., Montgomery, S.B., Chaib, H., Haddad, F., Snyder, M.P., 2020. Molecular choreography of acute exercise. Cell 181, 905349. https://doi.org/10.1016/j.cell.2020.04.043.
De Vos, S., Van Stappen, G., Sorgeloos, P., Vuylsteke, M., Rombauts, S., Bossier, P., 2019. Identification of salt stress response genes using the *Artemia* transcriptome. Aquaculture 500, 305–314. https://doi.org/10.1016/j.aquaculture.2018.09.067.
Domenech, F.A., 1980. Differentiation in Artemia in Spain. In: Persoone, G., Sorgeloos, P., Roels, O., Jaspers, E. (Eds.), The Brine Shrimp Artemia. Universa Press, Wetteren, pp. 19–39.
Dou, M., Jiao, Y.-H., Zheng, J.-W., Zhang, G., Li, H.-Y., Liu, J.-S., Yang, W.-D., 2020. De novo transcriptome analysis of the mussel *Perna viridis* after exposure to the toxic dinoflagellate *Prorocentrum lima*. Ecotoxicol. Environ. Saf. 192, 110265. https://doi.org/10.1016/j.ecoenv.2020.110265.
EFSA, 2008. Marine biotoxins in shellfish - okadaic acid and analogues - scientific opinion of the panel on contaminants in the food chain. EFSA Journal 6, 589. https://doi.org/10.2903/j.efsa.2008.589.
Escoffier, N., Gaudin, J., Mezhoud, K., Huet, H., Chateau-Joubert, S., Turquet, J., Crespeau, F., Edery, M., 2007. Toxicity to medaka fish embryo development of okadaic acid and crude extracts of Prorocentrum dinoflagellates. Toxicon 49, 1182–1192. https://doi.org/10.1016/j.toxicon.2007.02.008.
Ezraty, B., Gennaris, A., Barras, F., Collet, J.-F., 2017. Oxidative stress, protein damage and repair in bacteria. Nat. Rev. Microbiol. 15, 385–396. https://doi.org/10.1038/nrmicro.2017.26.
Feder, M.E., Hofmann, G.E., 1999. Heat-shock proteins, molecular chaperones and the stress response: evolutionary and ecology physiology. Annu. Rev. Physiol. 61, 243–282. https://doi.org/10.1146/annurev.physiol.61.1.243.
Ferron, P.J., Hogeveen, K., Fessard, V., Le Hégarat, L., 2014. Comparative analysis of the cytotoxic effects of okadaic acid-group toxins on human intestinal cell lines. Mar. Drugs 12, 4616–4634. https://doi.org/10.3390/md12084616.
Fu, L.L., Zhao, X.Y., Ji, L.D., Xu, J., 2019. Okadaic acid (OA): toxicity, detection and detoxification. Toxicon 160, 1–7. https://doi.org/10.1016/j.toxicon.2018.12.007.
Fujiki, H., Suganuma, M., 2009. Carcinogenic aspects of protein phosphatase 1 and 2A inhibitors. In: Fusetani, N., Kem, W. (Eds.), Marine Toxins as Research Tools. Springer Berlin Heidelberg, Berlin, Heidelberg, pp. 221–254, 2009.
Franchini, A., Casarini, L., Malagoli, D., Ottaviani, E., 2009. Expression of the genes siamois, engrailed-2, bmp4 and myf5 during Xenopus development in presence of the marine toxins okadaic acid and palytoxin. Chemosphere 308–312. https://doi.org/10.1016/j.chemosphere.2009.07.027.
Geng, N., Ren, X., Gong, Y., Zhang, H., Wang, F., Xing, L., Cao, R., Xu, J., Gao, Y., Giesy, J.P., Chen, J., 2019. Integration of metabolomics and transcriptomics reveals short-chain chlorinated paraffin-induced hepatotoxicity in male Sprague-Dawley rat. Environ. Int. 133, 105231. https://doi.org/10.1016/j.envint.2019.105231.
Gou, N., Gu, A.Z., 2011. A new transcriptional effect level Index (TELI) for toxicogenomics-based toxicity assessment. Environ. Sci. Technol. 45, 5410–5417. https://doi.org/10.1021/es200455p.
Guo, R., Ki, J.-S., 2013. Characterization of a novel catalase–peroxidase (KATG) gene from the dinoflagellate *Prorocentrum minimum*. J. Phycol. 49, 1011–1016. https://doi.org/10.1111/jpy.12094.
Gutner-Hoch, E., Martins, R., Maia, F., Oliveira, T., Shpigel, M., Weis, M., Tedim, J., Benayahu, Y., 2019. Toxicity of engineered micro- and nanomaterials with antifouling properties to the brine shrimp *Artemia salina* and embryonic stages of the sea urchin *Paracentrotus lividus*. Environ. Pollut. 251, 530–537. https://doi.org/10.1016/j.envpol.2019.05.031.
Huang, L., Zou, Y., Weng, H.-W., Li, H.-Y., Liu, J.-S., Yang, W.-D., 2015. Proteomic profile in *Perna viridis* after exposed to *Prorocentrum lima*, a dinoflagellate producing DSP toxins. Environ. Pollut. 196, 350–357. https://doi.org/10.1016/j.envpol.2014.10.019.
Hook, S.E., Osborn, H.L., Spadaro, D.A., Simpson, S.L., 2014. Assessing mechanisms of toxicant response in the amphipod *Melita plumulosa* through transcriptomic profiling. Aquat. Toxicol. 146, 247–257. https://doi.org/10.1016/j.aquatox.2013.11.001.
Jiang, M., 2011. Acute toxicity of okadaic acid to the embryonic development of egg and larvae of *Sparus microcephalus*. Asian J. Ecotoxicol. 6, 410–414 (*in Chinese with English abstract*).
Klein, J., 2000. Membrane breakdown in acute and chronic neurodegeneration: focus on choline-containing phospholipids. JNT (J. Neural Transm.) (8), 1027–1063. https://doi.org/10.1007/s007020070051.
Kozlowsky-Suzuki, B., Koski, M., Hallberg, E., Wallén, R., Carlsson, P., 2009. Glutathione transferase activity and oocyte development in copepods exposed to toxic phytoplankton. Harmful Algae 8, 395–406. https://doi.org/10.1016/j.hal.2008.08.025.
Landau, M., Miyamoto, G., Bolis, C., 1985. Growth and amino acid composition of *Artemia salina* (L. 1758) fed algae grown in different media (Anostraca). Crustaceana 49, 318–320. https://doi.org/10.1163/156854085X00657.
Lauritano, C., Carotenuto, Y., Procaccini, G., Turner, J.T., Ianora, A., 2013. Changes in expression of stress genes in copepods feeding upon a non-brevetoxin-producing strain of the dinoflagellate *Karenia brevis*. Harmful Algae 28, 23–30. https://doi.org/10.1016/j.hal.2013.05.004.
Lavarías, S., Heras, H., Pedrini, N., Tournier, H., Ansaldo, M., 2011. Antioxidant response and oxidative stress levels in *Macrobrachium borellii* (Crustacea: palaemonidae) exposed to the water-soluble fraction of petroleum. Comp. Biochem. Physiol. C Toxicol. Pharmacol. 153, 415–421. https://doi.org/10.1016/j.cbpc.2011.02.002.
Lee, J.-S., Igarashi, T., Fraga, S., Dahl, E., Hovgaard, P., Yasumoto, T., 1989. Determination of diarrhetic shellfish toxins in various dinoflagellate species. J. Appl. Phycol. 1, 147–152. https://doi.org/10.1007/BF00003877.
Leu, J.I.J., Pimkina, J., Frank, A., Murphy, M.E., George, D.L., 2009. A small molecule inhibitor of inducible heat shock protein 70. Mol. Cell 36, 15–27. https://doi.org/10.1016/j.molcel.2009.09.023.
Li, B., Dewey, C.N., 2011. RSEM: accurate transcript quantification from RNA-Seq data with or without a reference genome. BMC Bioinf. 12, 323. https://doi.org/10.1186/1471-2105-12-323.
Li, L., Ye, J., Ye, N., Huang, Y., 2011. Toxicity of red tide alga *Prorocentrum lima* Scherffel from Zhangjiang to a variety of fish, shrimp and shellfish. Fish. Sci. 30, 547–550 (*In Chinese with English abstract*).
Li, T., Li, E., Suo, Y., Xu, Z., Jia, Y., Qin, J.G., Chen, L., Gu, Z., 2017. Energy metabolism and metabolomics response of Pacific white shrimp *Litopenaeus vannamei* to sulfide toxicity. Aquat. Toxicol. 183, 28–37. https://doi.org/10.1016/j.aquatox.2016.12.010.
Li, X., Li, Z., Chen, J., Shi, Q., Zhang, R., Wang, S., Wang, X., 2014. Detection, occurrence and monthly variations of typical lipophilic marine toxins associated with diarrhetic shellfish poisoning in the coastal seawater of Qingdao City, China. Chemosphere 111, 560–567. https://doi.org/10.1016/j.chemosphere.2014.05.006.
Libralato, G., Prato, E., Migliore, L., Cicero, A.M., Manfra, L., 2016. A review of toxicity testing protocols and endpoints with *Artemia* spp. Ecol. Indicat. 69, 35–49. https://doi.org/10.1016/j.ecolind.2016.04.017.
Liu, N., Zhu, L., 2020. Metabolomic and transcriptomic investigation of metabolic perturbations in *Oryza sativa* L. triggered by three pesticides. Environ. Sci. Technol. 54, 6115–6124. https://doi.org/10.1021/acs.est.0c00425.
Liu, Z., Yu, P., Cai, M., Wu, D., Zhang, M., Huang, Y., Zhao, Y., 2019. Polystyrene nanoplastic exposure induces immobilization, reproduction, and stress defense in the freshwater cladoceran *Daphnia pulex*. Chemosphere 215, 74–81. https://doi.org/10.1016/j.chemosphere.2018.09.176.
Lloyd, J.K., Duchin, J.S., Borchert, J., Quintana, H.F., Robertson, A., 2013. Diarrhetic shellfish poisoning, Washington, USA, 2011. Emerg. Infect. Dis. 19, 1314–1316. https://doi.org/10.3201/eid1908.121824.
Lu, J., Tian, S., Lv, X., Chen, Z., Chen, B., Zhu, X., Cai, Z., 2018. TiO_2 nanoparticles in the marine environment: impact on the toxicity of phenanthrene and Cd^{2+} to marine zooplankton *Artemia salina*. Sci. Total Environ. 615, 375–380. https://doi.org/10.1016/j.scitotenv.2017.09.292.
Marcoval, M.A., Pan, J., Tang, Y., Gobler, C.J., 2013. The ability of the branchiopod, Artemia salina, to graze upon harmful algal blooms caused by *Alexandrium fundyense*, *Aureococcus anophagefferens*, and *Cochlodinium polykrikoides*. Estuarine. Coastal and Shelf Science 131, 235–244. https://doi.org/10.1016/j.ecss.2013.05.034.
Mello, D.F., Proença, L.A.D.O., Barracco, M.A., 2010. Comparative study of various immune parameters in three bivalve species during a natural bloom of *Dinophysis acuminata* in Santa Catarina Island, Brazil. Toxins 2, 1166–1178. https://doi.org/10.3390/toxins2051166.
Merzendorfer, H., Zimoch, L., 2003. Chitin metabolism in insects: structure, function and regulation of chitin synthases and chitinases. J. Exp. Biol. 206, 4393–4412. https://doi.org/10.1111/j.1558-5646.2008.00418.x.
Murray, I.M.T., Rowan, N.J., McNamee, S., Campbell, K., Fogarty, A.M., 2018. Pulsed light reduces the toxicity of the algal toxin okadaic acid to freshwater crustacean *Daphnia pulex*. Environ. Sci. Pollut. Control Ser. 25, 607–614. https://doi.org/10.1007/s11356-017-0472-6.
Nunes, B.S., Carvalho, F.D., Guilhermino, L.M., Van Stappen, G., 2006. Use of the genus Artemia in ecotoxicity testing. Environ. Pollut. 144, 453–462. https://doi.org/10.1016/j.envpol.2005.12.037.
Oakley, A., 2011. Glutathione transferases: a structural perspective. Drug Metabol. Rev. 43, 138–151. https://doi.org/10.3109/03602532.2011.558093.
Parvez, S., Raisuddin, S., 2006. Copper modulates non-enzymatic antioxidants in the freshwater fish *Channa punctata* (Bloch) exposed to deltamethrin. Chemosphere 62, 1324–1332. https://doi.org/10.1016/j.chemosphere.2005.07.025.
Poynton, H.C., Varshavsky, J.R., Chang, B., Cavigiolio, G., Chan, S., Holman, P.S., Loguinov, A.V., Bauer, D.J., Komachi, K., Theil, E.C., Perkins, E.J., Hughes, O., Vulpe, C.D., 2007. *Daphnia magna* ecotoxicogenomics provides mechanistic insights into metal toxicity. Environ. Sci. Technol. 41, 1044–1050. https://doi.org/10.1021/es0615573.

Prego-Faraldo, M.V., Vieira, L.R., Eirin-Lopez, J.M., Méndez, J., Guilhermino, L., 2017. Transcriptional and biochemical analysis of antioxidant enzymes in the mussel *Mytilus galloprovincialis* during experimental exposures to the toxic dinoflagellate *Prorocentrum lima*. Mar. Environ. Res. 129, 304–315. https://doi.org/10.1016/j.marenvres.2017.06.009.

Poynton, H.C., Loguinov, A.V., Varshavsky, J.R., Chan, S., Perkins, E.J., Vulpe, C.D., 2008. Gene expression profiling in *Daphnia magna* Part I: concentration-dependent profiles provide support for the no observed transcriptional effect level. Environ. Sci. Technol. 42, 6250–6256. https://doi.org/10.1021/es8010783.

Prado-Alvarez, M., Flórez-Barrós, F., Méndez, J., Fernandez-Tajes, J., 2013. Effect of okadaic acid on carpet shell clam (*Ruditapes decussatus*) haemocytes by in vitro exposure and harmful algal bloom simulation assays. Cell Biol. Toxicol. 29, 189–197. https://doi.org/10.1007/s10565-013-9246-1.

Reguera, B., Riobó, P., Rodríguez, F., Díaz, P.A., Pizarro, G., Paz, B., Franco, J.M., Blanco, J., 2014. Dinophysis toxins: causative organisms, distribution and fate in shellfish. Mar. Drugs 12, 394–461. https://doi.org/10.3390/md12010394.

Riisgård, H.U., Zalacáin, D., Jeune, N., Wiersma, J.B., Lüskow, F., Pleissner, D., 2015. Adaptation of the brine dhrimp *Artemia Salina* (Branchiopoda: Anostraca) to filter-feeding: effects of body size and temperature on filtration and respiration rates. J. Crustac Biol. 35, 650–658. https://doi.org/10.1163/1937240X-00002362.

Rocha, J., Garcia-Carreño, F.L., Muhlia-Almazán, A., Peregrino-Uriarte, A.B., Yépiz-Plascencia, G., Córdova-Murueta, J.H., 2012. Cuticular chitin synthase and chitinase mRNA of whiteleg shrimp *Litopenaeus vannamei* during the molting cycle. Aquaculture 330 (333), 111–115. https://doi.org/10.1016/j.aquaculture.2011.12.024.

Saibil, H., 2013. Chaperone machines for protein folding, unfolding and disaggregation. Nat. Rev. Mol. Cell Biol. 14, 630–642. https://doi.org/10.1038/nrm3658.

Savage, A., Knott, B., 1998. *Artemia parthenogenetica* in Lake Hayward, Western Australia. II. Feeding biology in a shallow, seasonally stratified, hypersaline lake. Int. J. Salt Lake Res. 7, 13–24. https://doi.org/10.1007/BF02449921.

Singh, S., Brocker, C., Koppaka, V., Chen, Y., Jackson, B.C., Matsumoto, A., Thompson, D.C., Vasiliou, V., 2013. Aldehyde dehydrogenases in cellular responses to oxidative/electrophilic stress. Free Radic. Biol. Med. 56, 89–101. https://doi.org/10.1016/j.freeradbiomed.2012.11.010.

Snyder, M.J., 2000. Cytochrome P450 enzymes in aquatic invertebrates: recent advances and future directions. Aquat. Toxicol. 48, 529–547. https://doi.org/10.1016/S0166-445X(00)00085-0.

Sokolova, I.M., Frederich, M., Bagwe, R., Lannig, G., Sukhotin, A.A., 2012. Energy homeostasis as an integrative tool for assessing limits of environmental stress tolerance in aquatic invertebrates. Mar. Environ. Res. 79, 1–15. https://doi.org/10.1016/j.marenvres.2012.04.003.

Song, Y., Rundberget, J.T., Evenseth, L.M., Xie, L., Gomes, T., Høgåsen, T., Iguchi, T., Tollefsen, K.E., 2016. Whole-organism transcriptomic analysis provides mechanistic insight into the acute toxicity of emamectin benzoate in *Daphnia magna*. Environ. Sci. Technol. 50, 11994–12003. https://doi.org/10.1021/acs.est.6b03456.

Souid, G., Souayed, N., Haouas, Z., Maaroufi, K., 2018. Does the phycotoxin Okadaic acid cause oxidative stress damages and histological alterations to seabream (*Sparus aurata*)? Toxicon 144, 55–60. https://doi.org/10.1016/j.toxicon.2018.02.001.

Sun, L., Wang, R., Ju, Q., Xu, J., 2020. Physiological, metabolic, and transcriptomic analyses reveal the responses of *Arabidopsis seedlings* to carbon nanohorns. Environ. Sci. Technol. 54, 4409–4420. https://doi.org/10.1021/acs.est.9b07133.

Torgersen, T., Miles, C.O., Rundberget, T., Wilkins, A.L., 2008. New esters of okadaic acid in seawater and blue mussels (*Mytilus edulis*). J. Agric. Food Chem. 56, 9628–9635. https://doi.org/10.1021/jf8016749.

Van Dolah, F.M., 2000. Marine algal toxins: origins, health effects, and their increased occurrence. Environ. Health Perspect. 108, 133–141. https://doi.org/10.2307/3454638.

Wang, F., Zhang, H., Geng, N., Ren, X., Zhang, B., Gong, Y., Chen, J., 2018. A metabolomics strategy to assess the combined toxicity of polycyclic aromatic hydrocarbons (PAHs) and short-chain chlorinated paraffins (SCCPs). Environ. Pollut. 234, 572–580. https://doi.org/10.1016/j.envpol.2017.11.073.

Wu, H., Chen, J., Peng, J., Zhong, Y., Zheng, G., Guo, M., Tan, Z., Zhai, Y., Lu, S., 2020. Nontarget screening and toxicity evaluation of diol esters of okadaic acid and dinophysistoxins reveal intraspecies difference of *Prorocentrum lima*. Environ. Sci. Technol. 54, 12366–12375. https://doi.org/10.1021/acs.est.0c03691.

Yan, T., Zhang, Y., Han, G., Chen, Y., Zhou, M., 2007. Experimental study on the harmful effects of large-scale HABs in the East China Sea - the toxicity to *Neomysis awatschensis* and Artemia *salina*. Stud. Mar. Sin. 48, 166–175 (*in Chinese with English abstract*).

Yasumoto, T., Oshima, Y., Yamaguchi, M., 1978. Occurrence of a new type of shellfish poisoning in the Tohoku District. Nippon Suisan Gakkaishi 44, 1249–1255. https://doi.org/10.2331/suisan.44.1249.

Yi, X., Zhang, K., Liu, R., Giesy, J.P., Li, Z., Li, W., Zhan, J., Liu, L., Gong, Y., 2019. Transcriptomic responses of *Artemia salina* exposed to an environmentally relevant dose of *Alexandrium minutum* cells or Gonyautoxin2/3. Chemosphere 238, 124661. https://doi.org/10.1016/j.chemosphere.2019.124661.

Young, N., Robin, C., Kwiatkowska, R., Beck, C., Mellon, D., Edwards, P., Turner, J., Nicholls, P., Fearby, G., Lewis, D., Hallett, D., Bishop, T., Smith, T., Hyndford, R., Coates, L., Turner, A., 2019. Outbreak of diarrhetic shellfish poisoning associated with consumption of mussels, United Kingdom, May to June 2019. Euro Surveill. 24, 1900513. https://doi.org/10.2807/1560-7917.ES.2019.24.35.1900513.

Zheng, F., Zhao, X., Zeng, Z., Wang, L., Lv, W., Wang, Q., Xu, G., 2020. Development of a plasma pseudotargeted metabolomics method based on ultra-high-performance liquid chromatography–mass spectrometry. Nat. Protoc. 15, 2519–2537. https://doi.org/10.1038/s41596-020-0341-5.

Zhu, S., Xue, M.Y., Luo, F., Chen, W.C., Zhu, B., Wang, G.X., 2017. Developmental toxicity of Fe_3O_4 nanoparticles on cysts and three larval stages of *Artemia salina*. Environ. Pollut. 230, 683–691. https://doi.org/10.1016/j.envpol.2017.06.065.

Supporting information for

Molecular mechanisms of zooplanktonic toxicity in the okadaic acid-producing dinoflagellate *Prorocentrum lima*

Yufeng Gong[1,2], Keke Zhang[1], Ningbo Geng[3], Minghuo Wu[1], ,Xianliang Yi[1,*], Renyan Liu[4,*] Jonathan K. Challis[2], Garry Codling[2,5], Elvis Genbo Xu[6], John P. Giesy[2,7,8,9]

[1] School of Ocean Science and Technology, Dalian University of Technology, Panjin Campus, Panjin, Liaoning, China

[2] Toxicology Centre, University of Saskatchewan, Saskatoon, SK, Canada

[3] CAS Key Laboratory of Separation Sciences for Analytical Chemistry, Dalian Institute of Chemical Physics, Chinese Academy of Sciences, Dalian, China

[4] National Marine Environmental Monitoring Center, Dalian, Liaoning, China

[5] RECETOX Centre, Masaryk University, Kamenice, Brno, Czech Republic

[6] Department of Biology, University of Southern Denmark, Odense, Denmark

[7] Department of Veterinary Biomedical Sciences, University of Saskatchewan, Saskatoon, SK, Canada

[8] Department of Environmental Sciences, Baylor University, Waco, Texas, USA

[9] State Key Laboratory of Pollution Control and Resource Reuse, School of the Environment, Nanjing University, Nanjing, People's Republic of China

***Corresponding Authors**

E-mail addresses: yixianliang@dlut.edu.cn (Xianliang Yi), ryliu@nmemc.org.cn (Renyan Liu).

Number of pages: 39

Number of figures: 12

Number of tables: 9

Contents:

1. Analysis of OA and its structural derivatives by HPLC-MS/MS

The exposure solutions were first filtered through 0.22 μm filter membrane and then subjected to solid phase extraction (SPE). The Strata^{TM}-X 33 μm Polymeric Reversed Phase cartridges were conditioned with 1 mL of methanol and equilibrated with 1 mL of 30% methanol in water. Then, 5 mL of filtrates were transferred to the top of the cartridges. The cartridges were washed with 1 mL of 20% methanol in water and subsequently eluted with 1.2 mL of methanol containing 0.3% ammonium hydroxide. The elution was collected for high-performance liquid chromatography-tandem mass spectrophotometry (HPLC-MS/MS) analysis.

A HPLC system (Dionex 3000, CA, USA) was coupled online to a triple quadrupole mass spectrometer (API4000 AB SCIEX, MA, USA). Chromatographic separation was carried out with a Waters X-Bridge C18 column (150 × 3.0 mm, 3.5 μm). Mobile phase A consisted of 0.05% (v/v) ammonia in water; mobile phase B consisted of 0.05% (v/v) ammonia in 90% acetonitrile with a flow rate set at 0.40 mL/min. Injection volume was set at 10 μL. Analyses were separated by gradient elution. Initial composition was 10% mobile phase B for 1.0 min, then increased to 90% in 9 min, maintained at 90% for 3 min, followed by a change to the initial condition in 2 min and re-equilibration at 10% mobile phase B for 4 min; total run time was 19 min. Temperature of column was set at 40 ℃. Mass spectra were acquired by the API 4000 MS/MS system equipped with electrospray ionization interface with turbo spray ion source. Ion spray voltage was set at −4500 V, and temperature was maintained at 600 ℃. Nebulizing gas was high-purity nitrogen, and gasses 1 and 2 were set at 60 and 50 L/min, respectively. Curtain and collision gasses were 13 and 5, respectively. Quantification was performed in multiple reactions monitoring (MRM)

mode with a dwell time of 125 ms for each transition. The mass spectrometric parameters for detection were listed in Table S1.

Table S1. Mass spectrometric parameters for detection

Target compound	Precursor ion (m/z)	Product ion (m/z)	DP (eV)	CE (eV)	EP (eV)
OA	803.5	255.1	-120	-62	-10
		563.2	-120	-62	-10
DTX1	817.5	255.2	-120	-62	-10
		577.2	-120	-62	-10
DTX2	803.5	255.2	-120	-62	-10
		577.2	-120	-62	-10
YTX	1141.5	1061.5	-60	-46	-12

2. Details for transcriptomics and qRT-PCR methods

Transcriptomisc analysis

Samples were homogenized with a pestle, and total RNA isolated by use of Trizol Reagent (Invitrogen Life Technologies). After checking integrity of RNA, three micrograms of RNA were used as input material for construction of a library. Due to contamination of RNA in one sample from the control group, a total of 11 sequence libraries were constructed, including 3 replicates in OA or *P. lima* exposure groups and 2 replicates in control group. Libraries of sequences were generated using the TruSeq RNA Sample Preparation Kit (Illumina, San Diego, CA, USA). The library was then sequenced on a Hiseq platform (Illumina) by Shanghai Personal Biotechnology Cp. Ltd.

Raw data in FASTQ format were first processed by Cutadapt (version 1.15) before *de novo* assembly. Clean reads were obtained by removing reads with an adaptor, low quality reads (< Q20) or reads with length less than 50 bp. Then, clean reads with high quality were assembled using Trinity software (r20140717, K-mer 25 bp) to construct transcript and unigene sequences. Afterwards, assembled unigenes were annotated for function against several public databases, including the NCBI non-redundant protein sequences (NR) database, Gene Ontology (GO) database, Kyoto Encyclopedia of Genes and Genome (KEGG) database, evolutionary genealogy of genes: Non-supervised Orthologous Groups (eggNOG) database and Swiss-Prot database with a threshold E-value $\leq 1e^{-5}$ according to Conesa et al. (2005)[1]. Clean reads were mapped to each assembled unigene by RSEM software[2]. Transcript abundances were measured as Fragments per kilobase of transcript sequence per millions base pairs sequenced (FPKM). The transcriptomics data was validated through quantitative real time PCR (qRT-PCR). Eight unigenes were randomly

selected and housekeeping glyceraldehyde-3-phosphate dehydrogenase (GAPDH) was employed as the reference gene.

qRT-PCR validation

Eight genes were randomly selected for confirmation of transcriptomics data by using quantitative real time PCR (qRT-PCR). Primer sequences were listed in Table S2. Sequences of these selected unigenes were compared with the homologues (blastx) to verify our annotation. RNA samples of *A. salina* were extracted with the same method as described in transcriptomics analysis, and concentrations of RNA were determined with Nanodrop 2000 (Thermo Scientific, USA). Two micrograms of isolated RNA was applied for complimentary DNA (cDNA) synthesis with a Universal RT-PCR Kit (Solarbio, China), and 2 μL of cDNA templates were applied in each reaction. The RT-PCR were carried out on a 7500 RT-PCR systems (Applied Biosystems, USA). Glyceraldehyde-3-phosphate dehydrogenase (GAPDH) was adopted as the reference gene. Reaction conditions were: 95 ℃/ 4 min, 40 cycles of 95 ℃/15 s, 60 ℃/30 s and 72 ℃/30 s. Melting curves were determined with: 5 ℃/1 min, and 80 cycles of 65 ℃/5 s with 0.5 ℃ increase per cyle. Relative expression of the target genes were calculated by $2^{-\Delta\Delta Ct}$ method[3].

Table S2. Primer sequences used in qRT-PCR analysis

Unigene name	NR database annotation	Primer sequences (5' → 3')
c14124_g1	Proteasome subunit beta type-2	F: GTATATCGCCTTCCCTGACGC
		R: GCAGATAGCTACAGCTACGGAC
c57652_g1	Phosphoserine aminotransferase 1	F: GCTATGTGCACTACTGCGAC
		R: CTTCAGCTCGTTGTACTGCG
c167662_g1	Serine--pyruvate aminotransferase	F: CTTCAGCTCGTTGTACTGCG
		R: GCGTCATAGCGTGCTGGTTGTG
c182641_g1	Cytochrome c oxidase subunit 1	F: CGGAGCCCCAGATATAGCATTC
		R: GACAGTGTTTCATGTGGTGTAAGC
c220604_g2	Trypsin-1	F: GCTGACACTGTTTTGACTGCTGC
		R: GAACGTGATCACCGGCAACAAC
c210472_g1	Phosphoglycerate kinase	F: GGCTGAAGAACTCAGAAAGC
		R: CGAGCTGTAGCATCTACAGC
c216620_g1	Aspartate aminotransferase, cytoplasmic	F: CAGTAGCCTTAGCTGCTCCAATCG
		R: CATTGTCAAGATCTCCTGATGC
c225143_g1	Tyrosine aminotransferase	F: CTGCAGTGGTTGTTCCTGTGC
		R: CATGCATTGGCTGCGATCATTC

Glyceraldehyde-3-phosphate dehydrogenase (GAPDH) was employed as housekeeping gene. The primer sequences (5'→3') were F: GTTGATGGCAAACTCGTCATA; R: CCACCTTCCAAGTGAGCATTA, according to Chen and Ge (2009)[4].

3. Sample preparation and instrumental analysis for metabolomics

Sample preparation

Sample was mixed with 1 mL of ultrapure water, homogenized, and then ultrasonically disrupted for 5 min in an ice-water bath. The sample were subsequently freeze-dried and extracted with a mixture of methanol/water (4: 1, v: v). Soon afterwards, the solution was vortexed for 30 min, and then centrifuged for 20 min at 13,000 × g and 4 ℃. Finally, the supernatant was filtered by an organic phase filter and transferred to a vial for metabolite analysis. Prior to extraction, six kinds of internal standards (i.e., L-phenylalanine-d5, octanoyl (8,8,8-d3)-L-carnitine, 1-lauroyl-2-hydroxy-sn-glycero-3-phosphocholine, 1,2-diheptadecanoyl-sn-glycero-3-phosphoethanolamine, hendecanoic acid, and nonadecanoic acid) were spiked into the sample for the purpose of quality control.

UHPLC/Q-TOF MS for Untargeted Tandem MS

For untargeted tandem MS, the "auto MS/MS" function of the Q-TOF MS system with data-dependent acquisition was performed in positive ion mode and negative ion mode, respectively. For positive ion mode, 5 μL of extract containing metabolites was injected into the UHPLC/Q-TOF MS system with an ACQUITY UPLC BEH C8 column (2.1 mm × 100 mm × 1.7 μm, Waters, USA) maintained at 50 °C. Water and acetonitrile both containing 0.1% (v/v) formic acid were used as mobile phases A and B, respectively. The flow rate was 0.35 mL/min, and the gradient elution was as follows (time, %B): 0 min, 10%; 3 min, 40%; 15 min, 100%, and maintained for 5 min; 20.1 min, 10%, and re-equilibrated for 2.9 min. The mass spectrometer was operated with a capillary voltage of 4000 V, fragmentor voltage of 175 V, skimmer voltage of 65 V, nebulizer gas (N_2) pressure

at 45 psi, drying gas (N_2) flow rate of 9 L/min, and a temperature of 350 ℃. Five most intense precursors were chosen within one full scan cycle (0.25 s) with a precursor ion scan range of m/z 100−1000 and a tandem mass scan range of m/z 40−1000. The collision energies were set at 10, 20, 30, and 40 eV, and all samples were analyzed to obtain abundant and complementary product ion information.

For negative ion mode, 5 μL of extract containing metabolites was injected into the UHPLC/Q-TOF MS system with an ACQUITY UPLC HSS T3 column (2.1 mm × 100 mm × 1.8 μm, Waters, USA) maintained at 50 ℃. Water and methanol both containing 5 mmol/L ammonium bicarbonate were used as mobile phases A and B, respectively. The flow rate was also 0.35 mL/min, and the gradient elution was as follows (time, %B): 0 min, 2%; 3 min, 42%; 12 min, 100%, and maintained for 4 min; 16.1 min, 2%, and re-equilibrated for 3.9 min. The mass spectrometer was operated with a capillary voltage of 3500 V, fragmentor voltage of 175 V, skimmer voltage of 65 V, nebulizer gas (N_2) pressure at 45 psi, drying gas (N_2) flow rate of 9 L/min, and a temperature of 350 ℃. Five most intense precursors were chosen within one full scan cycle (0.25 s) with a precursor ion scan range of m/z 100−1000 and a tandem mass scan range of m/z 40−1000. The collision energies were set at −10, −20, −30, and −40 eV, and all samples were analyzed to obtain abundant and complementary product ion information.

After data acquisition, the “Find by Auto MS/MS” function of MassHunter Qualitative Analysis software was used to automatically extract ion pair information for subsequent MRM detection. The retention time window was set to 0.15 min; the MS/MS threshold was set to 100, and the mass match tolerance was set to 0.02 Da. The single mass expansion was set to symmetric 100 ppm, and the persistent background ions, such as

reference mass ions, were excluded. After execution, detected ion pairs with information about the precursor ion, product ions, retention time, and collision energy were exported to a spreadsheet. Ion pairs were selected on the basis of the following rules: different precursor ions eluted in the neighboring time range were scrutinized to exclude the isotopic, fragmentation, adduct, and dimer ions; and the product ion that appeared with the most applied collision energy and with the highest intensity was selected as the characteristic product ion.

UHPLC/Q-Trap MRM MS for Pseudo-targeted Metabolomic Analysis

A Waters Acquity Ultra Prerformance liquid chromatography system (UHPLC) coupled online to an ABI Q-Trap 5500 (AB SCIEX, USA) via an electrospray ionization (ESI) interface was adopted for pseudo-targeted metabolomics analysis using the spreadsheet produced from the analysis of UHPLC/Q-TOF MS. The same chromatographic condition, including chromatographic column, mobile phases, and gradient elution procedure, was performed on both UHPLC/Q-TOF MS system and UHPLC/Q-Trap MS system.

For positive ion mode, The MS instrumental parameters were set as those for the following: source temperature, 550 ℃; gas I, 40 arbitrary units; gas II, 40 arbitrary units; curtain gas, 35 arbitrary units; ion spray voltage, 5500 V.

For negative ion mode, The MS instrumental parameters were set as follows: source temperature, 550 ℃; gas I, 40 arbitrary units; gas II, 40 arbitrary units; curtain gas, 35 arbitrary units; ion spray voltage, −4500 V.

4. Determination of transcriptional effect level index (TELI)

TELI converts the information-rich toxicogenomic data into an integrated endpoint index, that can represent overall alteration of transcriptions alteration[5]. The TELI considers and incorporates three factors: (1) the number and identify of genes that exhibited altered expression, (2) the magnitude of altered gene expression for each gene response to the exposure, and (3) the time factor. Here, a single duration of exposure was used for all treatments so it can be set to a constant unity value of 1.0. Thus, the TELI value was calculated using the following equation:

$$\mathrm{TELI}_{(\mathrm{genei})} = e^{|\ln(\mathrm{I})|} - e^{|\ln(1)|} \qquad \text{(Equation 1)}$$

$$\mathrm{TELI}_{(\mathrm{total})} = \sum_{\mathrm{gene\ (i=1)}}^{\mathrm{genei\ (i=n)}} (\mathrm{TELI}_{\mathrm{genei}}) \qquad \text{(Equation 2)}$$

Where, I is the gene expression change; i is the number of genes in the transcriptomics data, and control gene expression level (I = 1) is subtracted from each data point.

5. Summary statistics of transcriptome sequencing

Table S3. Summary statistics of transcriptome sequencing of *A. salina* from control group (Control1 and 2), 4 μg/L of Okadaic acid exposure group (OA_L 1-3), 20 μg/L of Okadaic acid exposure group (OA_H 1-3) and *P. lima* exposure group (PL1-3)

Sample name	Raw reads	Clean reads	Clean bases	Q30 (%)	GC content (%)	Transcript number	Unigene number	Mean length of unigenes (bp)
Control1	47,124,796	46,641,062	6.93G	93.26	40.22	570,791	474,366	477.1
Control2	46,183,910	45,880,374	6.82G	94.91	40.27			
OA_L1	41,842,300	41,571,476	6.18G	94.97	40.39			
OA_L2	46,010,870	45,605,584	6.78G	93.72	40.6			
OA_L3	43,451,438	43,087,322	6.39G	94.02	40.7			
OA_H1	45,546,454	45,221,102	6.71G	94.99	41.02			
OA_H2	42,515,386	42,201,172	6.24G	95.15	41.11			
OA_H3	46,548,028	46,188,838	6.86G	94.22	40.8			
PL1	40,954,966	40,550,148	6.01G	93.57	40.77			
PL2	42,930,694	42,614,558	6.29G	95.23	41.04			
PL3	45,640,670	45,359,984	6.71G	95.16	40.83			

6. Annotation of unigenes

Table S4. Annotation of unigenes in different databases

Databases	Number of annotated unigenes	Percentage (%)
NR	48,186	10.16
GO	126,811	26.73
KEGG	4,721	0.99
eggNOG	56,373	11.88
Swissprot	37,667	7.94
In all database	2,841	0.60

7. Alignment statistics of the *A. salina* transcriptome against NR databases

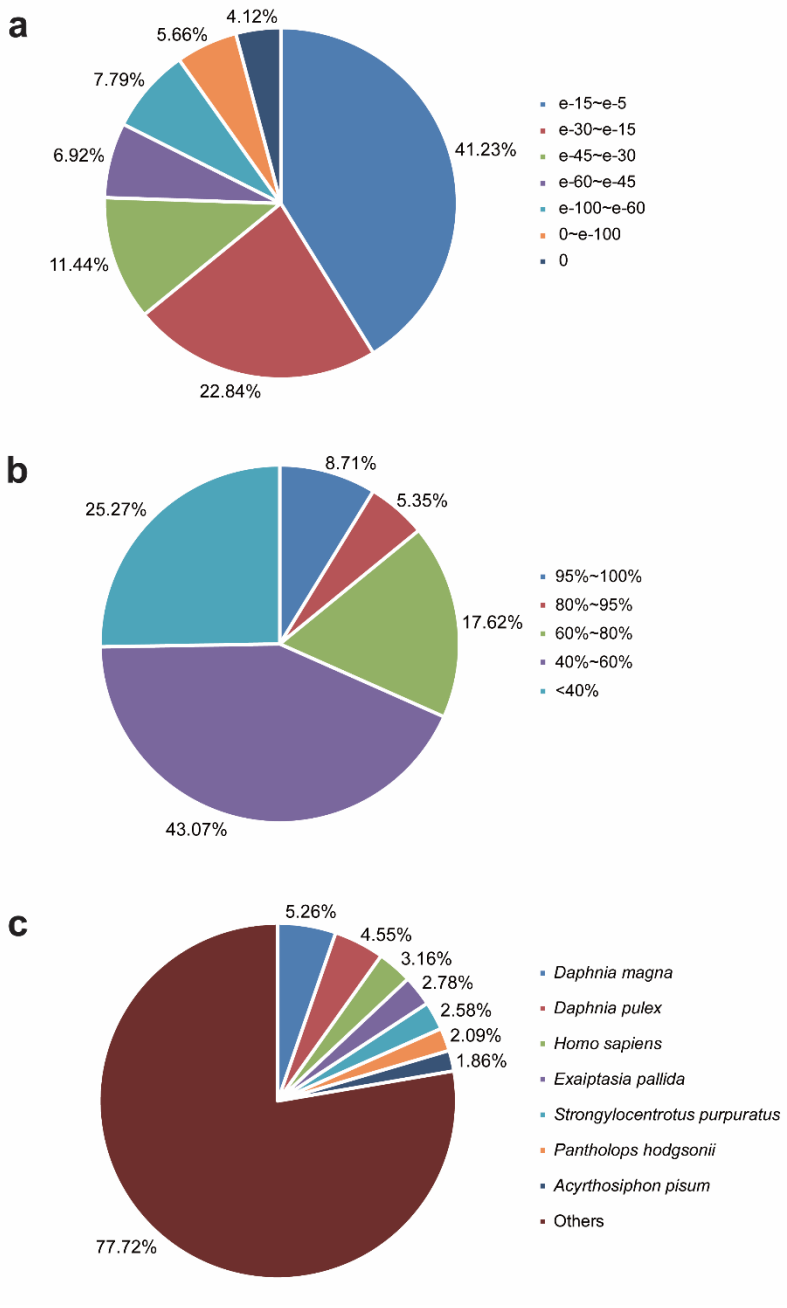

Figure S1. Alignment statistics of the transcriptome against NR databases. (a) *E*-value distribution; (b) Similarity distribution; and (c) Species distribution.

8. KEGG classification of *A. salina* transcriptome into functional groups

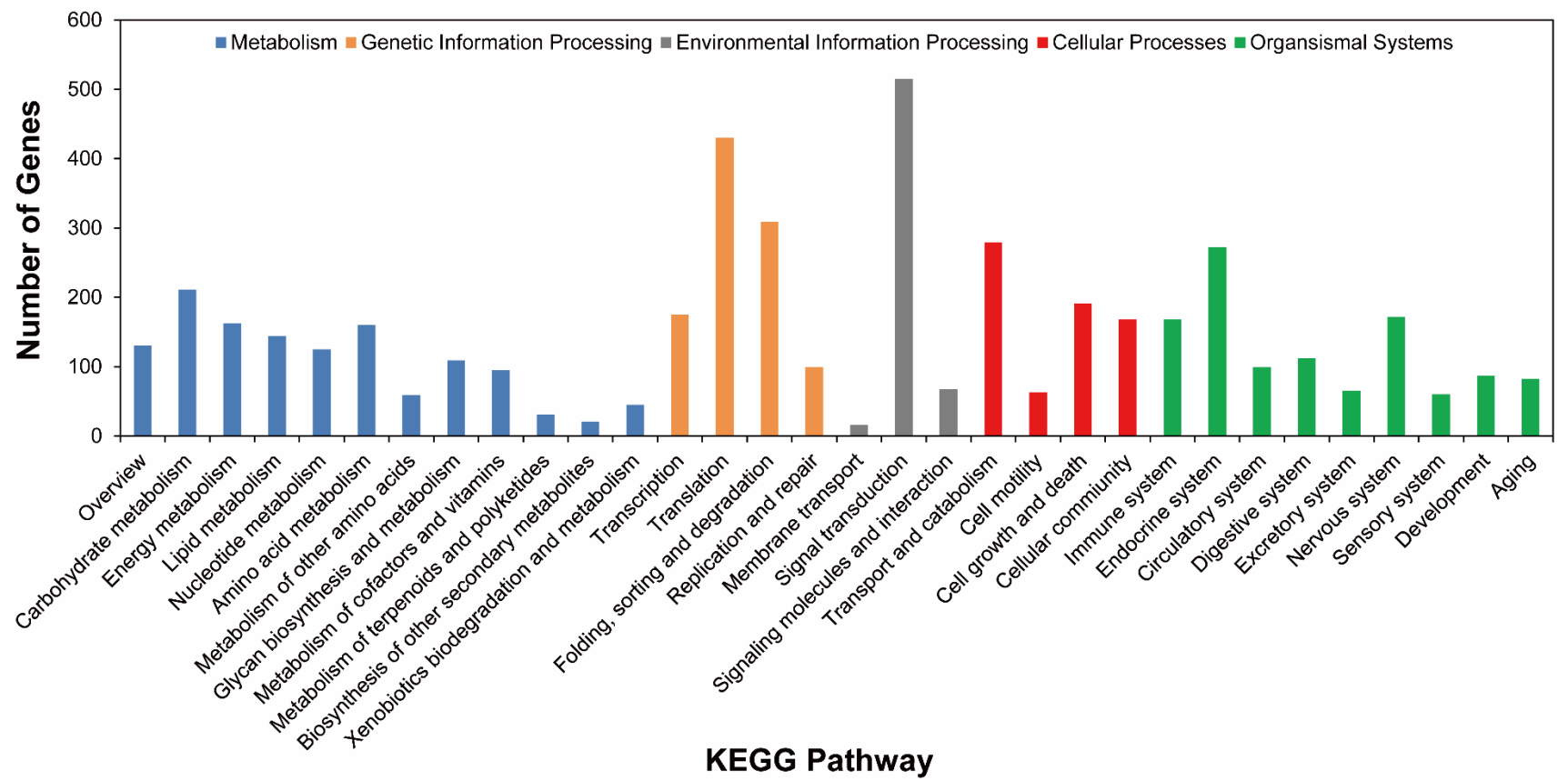

Figure S2. KEGG classification of *A. salina* transcriptome into functional groups.

9. GO terms distribution of annotated unigenes in *A. salina*

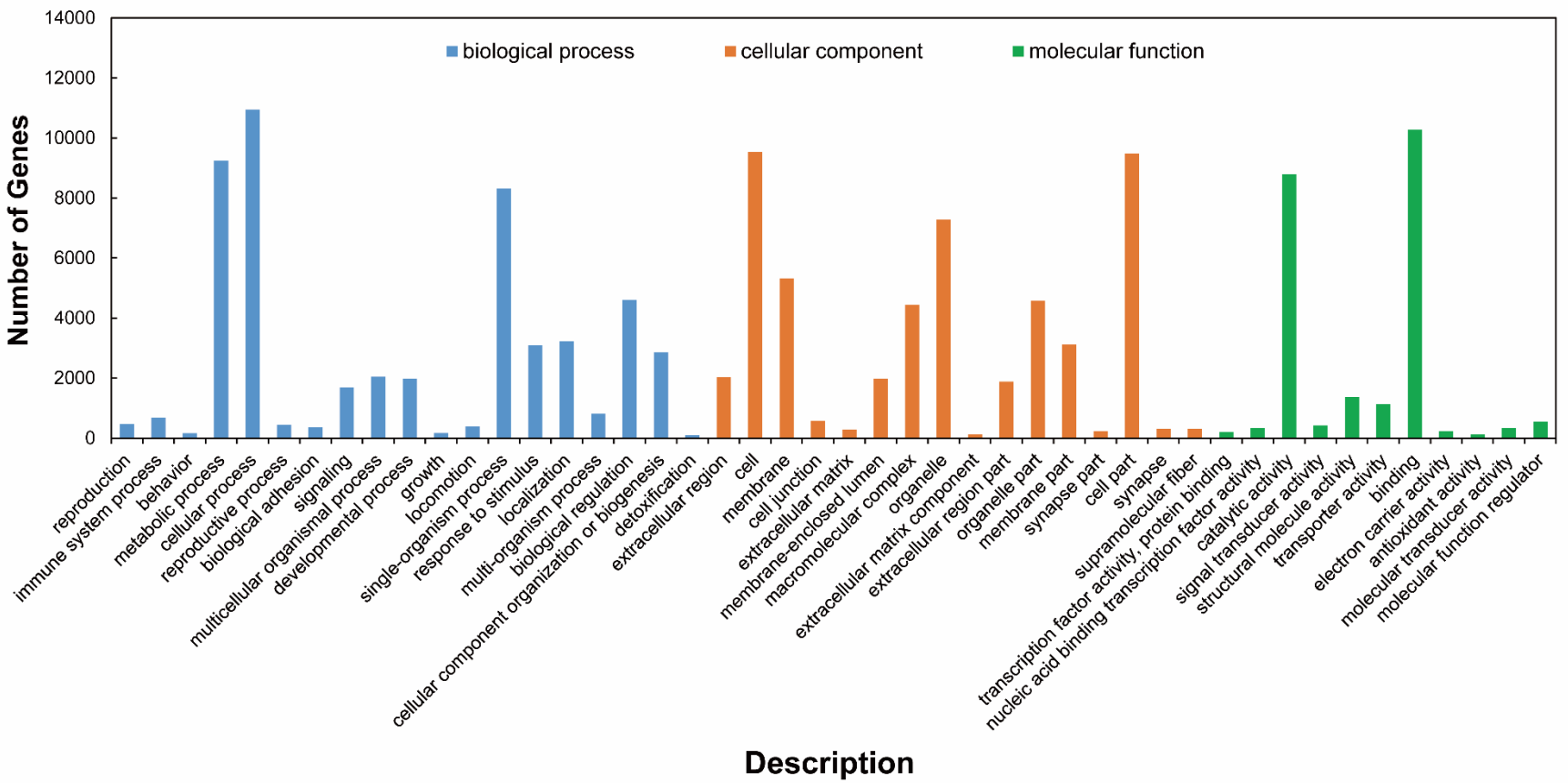

Figure S3. GO terms distribution of annotated unigenes in *A. salina*.

10. Overlap of DEGs / DMs among the three exposure groups

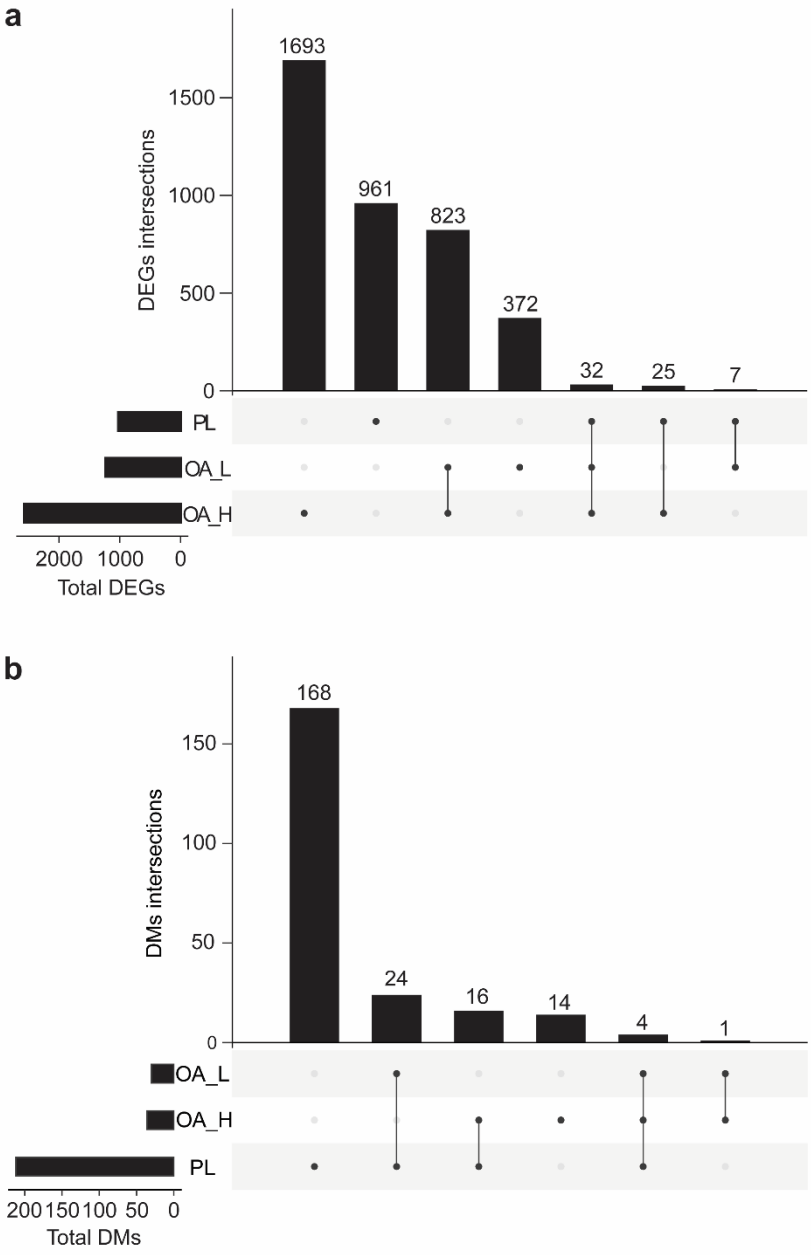

Figure S4. Upset plot showing the overlaps of DEGs (a) and DMs (b) among the three exposure groups. The plot was produced by UpsetR package. OA_L: 4 μg/L of OA exposure group; OA_H: 20 μg/L of OA exposure group; PL: 1.5×10^3 cell/L of *P. lima* exposure group.

11. Fold change (FC) distribution of DEGs

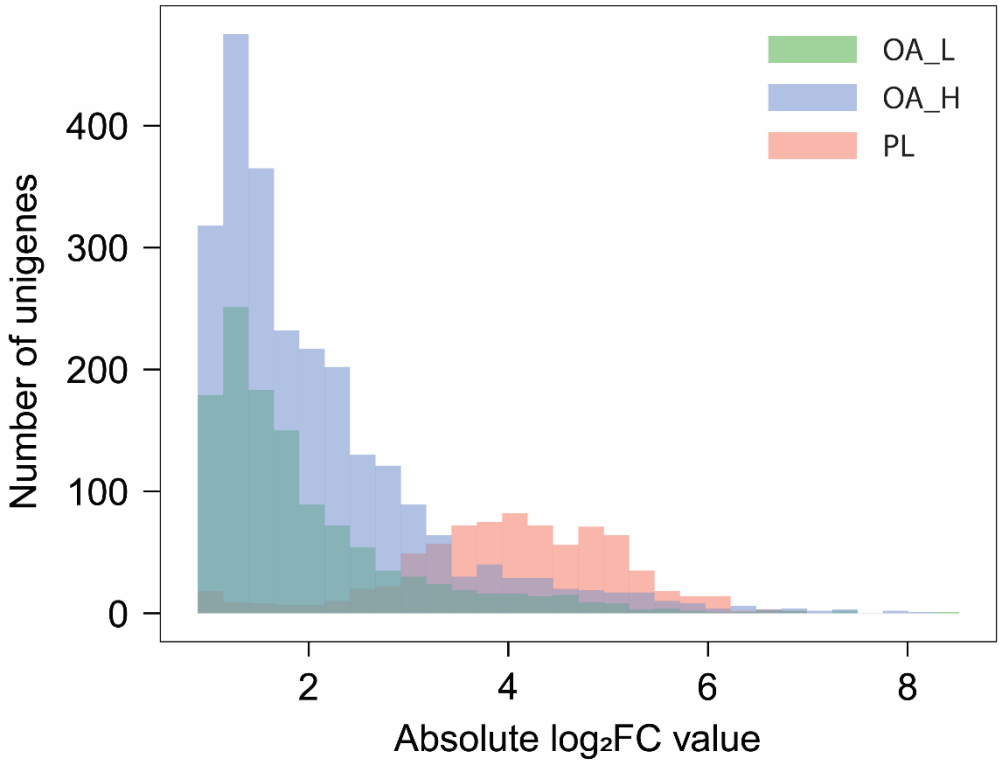

Figure S5. Fold change distribution of DEGs. DEGs were identified with the criteria of *P* value < 0.05 and |FC| > 2 in adult *A. salina* after exposure to 4 μg/L of OA (OA_L), 20 μg/L of OA (OA_H), or 1.5×10^3 of *P. lima* (PL).

12. Significantly enriched GO terms of DEGs

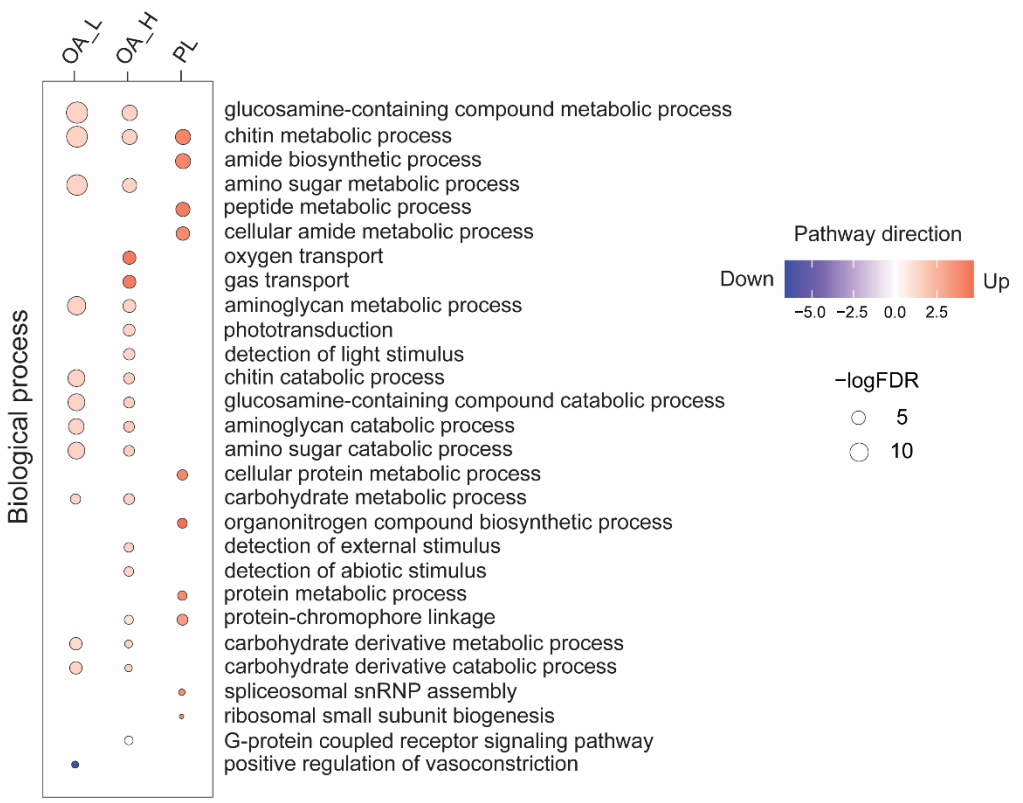

Figure S6. Significantly enriched GO biological process (BP) terms of differentially expressed genes (DEGs) in *A. salina* after exposure. Pathway direction is the median log2 fold change relative to control of DEGs in each pathway (blue, downregulated; red, upregulated). *P* values were corrected for multiple hypothesis by Benjamini-Hochberg method and GO terms with FDR < 0.05 were treated as significant. The dot size represents pathway significance.

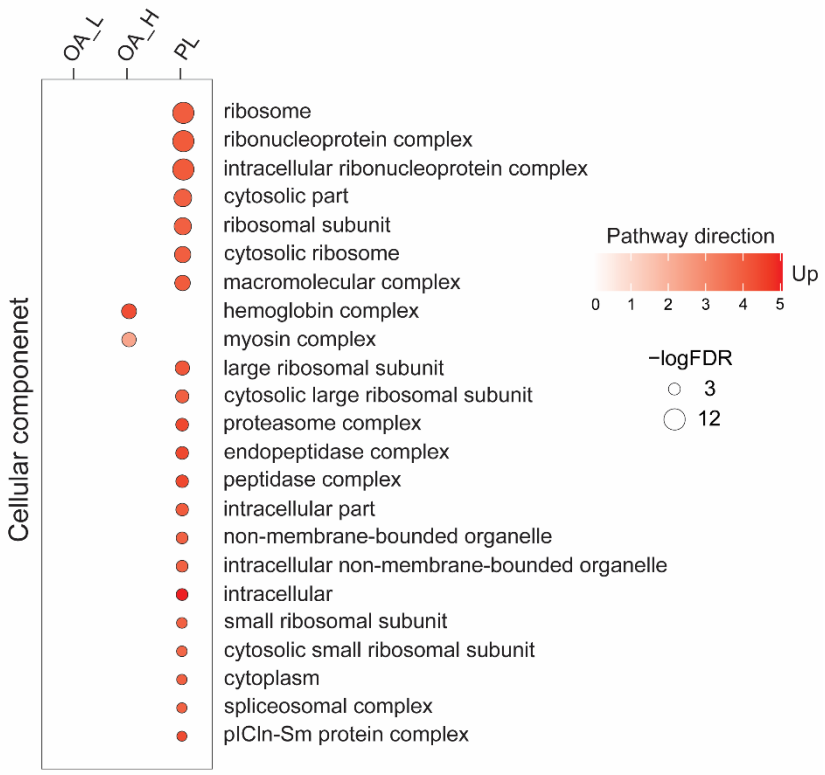

246

247 **Figure S7.** Significantly enriched GO cellular component (CC) terms of differentially
248 expressed genes (DEGs) in *A. salina* after exposure. Pathway direction is the median log2
249 fold change relative to control of DEGs in each pathway (blue, downregulated; red,
250 upregulated). *P* values were corrected for multiple hypothesis by Benjamini-Hochberg
251 method and GO terms with FDR < 0.05 were treated as significant. The dot size represents
252 pathway significance.

253

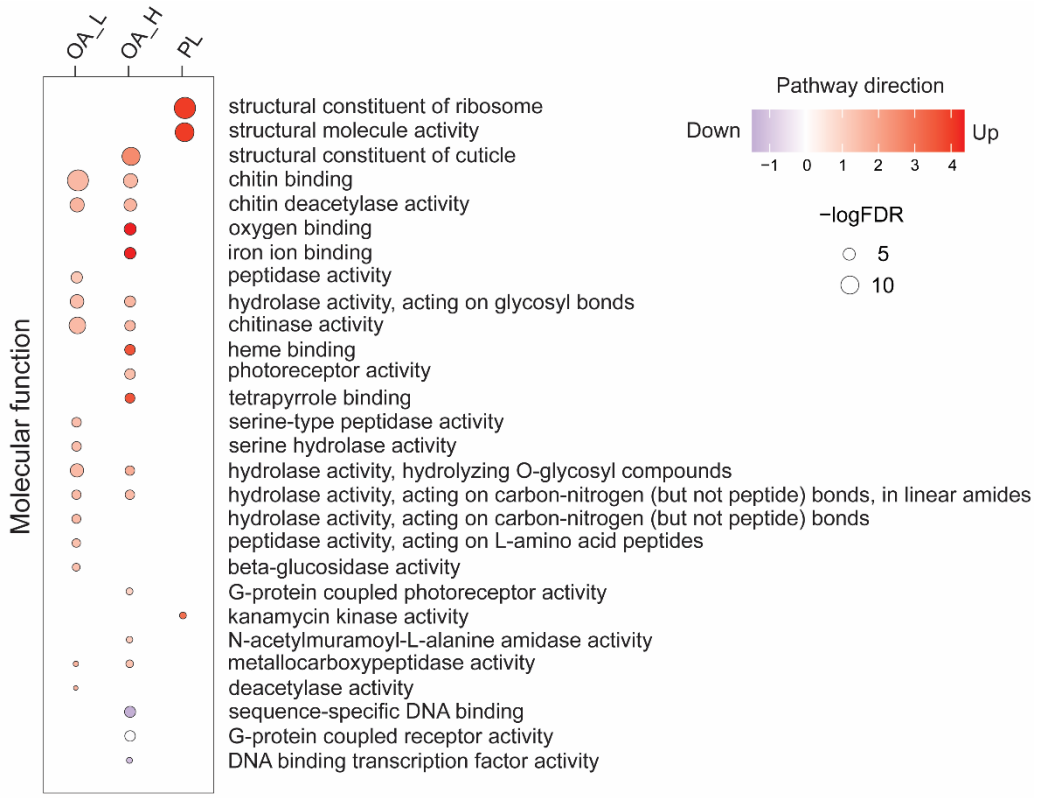

Figure S8. Significantly enriched GO molecular function (MF) terms of differentially expressed genes (DEGs) in *A. salina* after exposure. Pathway direction is the median log2 fold change relative to control of DEGs in each pathway (blue, downregulated; red, upregulated). *P* values were corrected for multiple hypothesis by Benjamini-Hochberg method and GO terms with FDR < 0.05 were treated as significant. The dot size represents pathway significance.

13. RT-PCR validation of transcriptomics data

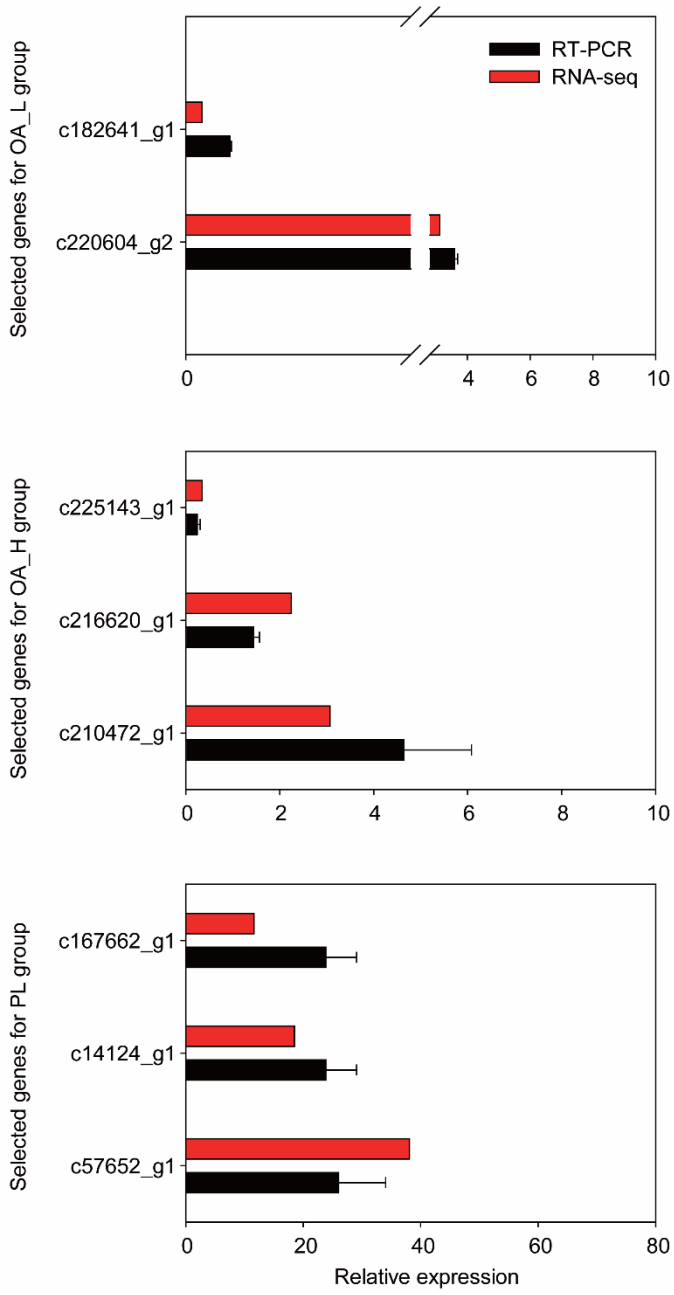

Figure S9. RT-PCR validation of selected genes of *A. salina* in OA_L, OA_H or PL groups. Bar indicated the average fold change of a selected unigene in exposure group relative to the control.

14. Reproducibility of metabolomics analysis

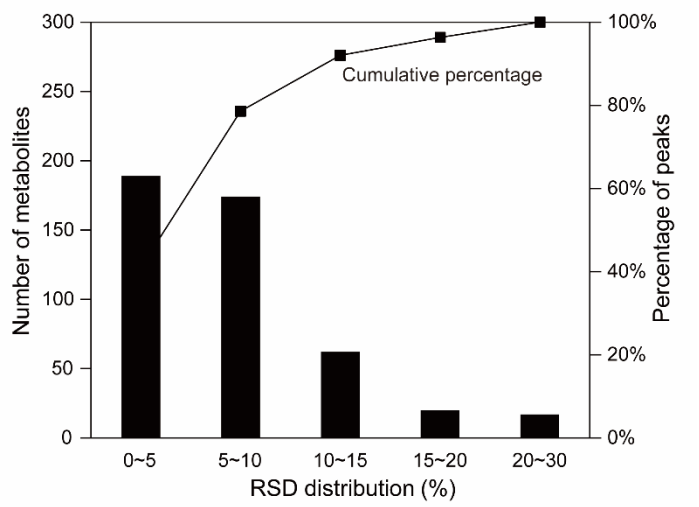

Figure S10. Reproducibility of pseudo-targeted metabolomics analysis for pooled QC. RSD: relative standard deviation.

15. Confidentially annotated DMs in *A. salina* after exposure

Table S5. Confidentially annotated DMs

Metabolites[1]	f.value	FDR	Log_2(fold change)		
			Exposure groups[2]		
			OA_L	OA_H	PL
3-Phosphoglycerate	16.648	0.002	0.550	0.171	0.765
Acetyl-CoA	10.221	0.006	-0.412	0.116	-1.412
Alanine	7.720	0.011	0.110	0.216	-0.391
Ascorbic acid	9.939	0.006	0.277	0.101	-0.994
Carnitine	8.691	0.009	0.146	0.065	0.652
Acylcarnitine C12:0	7.718	0.011	-0.094	-0.302	-0.765
Acylcarnitine C14:0	8.027	0.011	-0.088	-0.198	-0.685
Acylcarnitine C14:1	4.795	0.038	-0.131	-0.449	-0.669
Acylcarnitine C16:0	10.578	0.006	-0.082	0.086	-0.382
Acylcarnitine C16:2	6.702	0.016	-0.065	-0.127	-0.756
Acylcarnitine C18:2	6.898	0.015	0.061	0.274	-0.813
Acetylcarnitine	4.392	0.048	0.500	0.575	0.641
Choline	4.678	0.041	0.214	0.390	0.730
Glycerophosphocholine	8.697	0.009	0.141	-1.163	-0.683
Citric acid	4.425	0.048	0.676	0.499	-0.662
Cytidine	17.120	0.002	-0.404	-1.176	0.036
Deoxycytidine	13.611	0.003	-0.596	-1.353	0.529
Fructose 6-phosphate	4.482	0.046	0.949	0.922	0.258
FFA 15:0	9.339	0.007	-0.020	0.186	-0.679
FFA 17:1	5.925	0.023	0.050	0.068	-0.246
FFA 20:1	12.919	0.003	0.127	-0.221	0.732
FFA 22:1	8.182	0.010	0.172	-0.246	0.977
FFA 22:5	6.394	0.018	-0.020	-0.086	-0.685
FFA 22:7	9.181	0.007	0.112	-0.248	0.755
FFA 24:0	10.963	0.005	0.163	-0.260	0.848
FAA C18:1	7.743	0.011	0.518	-0.162	1.589
FAA C20:1	5.019	0.034	-0.039	-0.379	0.929
FAA C22:1	7.164	0.014	-0.067	-0.410	1.067
Glycine	5.737	0.024	0.104	0.013	-0.387

Guanosine triphosphate	14.314	0.003	0.015	0.535	-0.731
Indoleacrylic acid	9.408	0.007	0.152	0.201	-1.181
Isoleucine	13.095	0.003	0.038	-0.117	0.406
Aspartic acid	12.515	0.003	0.199	0.224	-1.119
Malic acid	10.439	0.006	0.531	1.262	-0.475
LPC 14:0	7.949	0.011	-0.142	0.142	-1.521
LPC 15:0	7.436	0.012	-0.003	0.451	-0.983
LPC 16:1	4.391	0.048	-0.028	0.255	-0.426
LPC 18:1	20.832	0.002	0.001	0.543	-1.044
LPC 18:2	10.892	0.005	-0.211	0.245	-1.424
LPC 18:3	14.896	0.003	-0.047	0.443	-0.833
LPC 20:2	7.801	0.011	0.091	0.463	-0.562
LPC 20:5	5.270	0.030	-0.064	0.300	-0.853
LPC 22:6	7.176	0.014	-0.050	0.195	-1.053
LPC O-18:0	23.827	0.002	0.086	0.865	-0.653
LPE 16:0	5.311	0.029	0.215	0.859	-0.268
LPE 18:1	5.512	0.027	0.141	0.108	-0.281
LPE 18:2	6.211	0.020	-0.317	-0.334	-1.030
Threonine	4.800	0.038	0.113	0.036	-0.347
Methylstearate	5.756	0.024	-0.221	-0.304	0.594
Dimethylglycine	6.514	0.017	0.169	0.320	0.801
Orotidine-5-phosphate	8.666	0.009	0.169	-0.112	0.362
PC(30:1)	6.817	0.016	-0.169	-0.061	-0.649
PC(31:0)	7.132	0.014	0.184	0.386	-0.287
PC(32:4)	9.572	0.007	-0.342	-0.291	-1.031
PC(33:1)	4.380	0.048	0.133	0.244	-0.266
PC(36:6)	6.276	0.019	-0.362	-0.281	-0.848
PC(38:7)	8.481	0.009	-0.150	-0.132	-0.718
Phenylalanine	17.660	0.002	0.057	-0.073	0.468
Sarcosine	7.848	0.011	0.155	0.222	-0.311
Serotonin	4.859	0.037	0.064	0.568	0.058
SM(d18:1/15:0)	39.045	0.000	-0.238	0.241	-0.710
SM(d18:1/16:0)	14.427	0.003	-0.253	-0.112	-0.489
SM(d18:1/16:0)(OH)	11.206	0.005	-0.154	0.127	-0.540
SM(d18:1/16:1)	12.474	0.003	-0.339	-0.038	-0.537

5'-Methylthioadenosine	4.316	0.050	0.492	0.548	0.827
Uric acid	8.573	0.009	0.496	0.746	-0.870
Urea	11.678	0.004	0.210	0.069	0.809
Uridine	4.628	0.042	0.713	0.722	-0.357
Valine	5.579	0.026	0.079	0.148	-0.490

274 FFA: free fatty acid; FAA: fatty acid amide; LPC O: ether-linked lysophosphatidylcholine; LPC:
275 lysophosphatidylcholine; LPE: lysophosphatidylethanolamine; PC: Phosphatidylcholine; SM:
276 sphingomyelin.
277 OA_L: 4 μg/L of OA exposure group; OA_H: 20 μg/L of OA exposure group; PL: 1.5×10^3 cell/L of
278 *P. lima* exposure group.
279

16. Actual concentrations of OA and its structural derivatives in exposure solutions

Table S6. Actual concentrations of OA and its analogs in exposure solutions measured by targeted LC-MS/MS analysis (μg/L, $N = 3$)

Exposure group	Concentrations measured by LC-MS/MS			
	OA	DTX1	DTX2	YTX
OA_L	5.10 ± 0.07	ND	ND	ND
OA_H	20.85 ± 0.40	ND	ND	ND
PL	9.83 ± 1.56	5.47 ± 0.49	ND	ND
400 μg/L OA	415.35 ± 7.63	ND	ND	ND

OA_L: 4 μg/L of OA exposure group; OA_H: 20 μg/L of OA exposure group; PL: 1.5×10^3 cells/L of *P. lima* exposure group. ND: not detected; 400 μg/L OA: the highest exposure concentration in acute toxicity test, and the other exposure concentrations in acute tests were prepared by series dilution.

17. KEGG enrichment analysis of DEGs

Table S7. KEGG enrichment results

Pathway ID	Pathway	Up num.	Down num.	Total num.	*P*-value	FDR
OA_L vs Control						
ko00500	Starch and sucrose metabolism	4	0	21	0.001	0.036
OA_H vs Control						
ko00010	Glycolysis / Gluconeogenesis	10	1	36	0.000	0.001
ko00500	Starch and sucrose metabolism	6	1	21	0.000	0.008
ko00400	Phenylalanine, tyrosine and tryptophan biosynthesis	2	1	3	0.000	0.008
ko00360	Phenylalanine metabolism	2	2	7	0.000	0.010
ko04512	ECM-receptor interaction	5	0	12	0.000	0.010
ko00981	Insect hormone biosynthesis	2	2	9	0.001	0.027
ko04080	Neuroactive ligand-receptor interaction	1	6	31	0.002	0.037
PL vs Control						
ko03050	Proteasome	6	0	41	0.000	0.003
ko03040	Spliceosome	9	0	121	0.000	0.003
ko00680	Methane metabolism	4	0	16	0.000	0.003
ko00260	Glycine, serine and threonine metabolism	4	0	23	0.000	0.007
ko03010	Ribosome	9	0	178	0.001	0.016
ko04612	Antigen processing and presentation	3	0	17	0.002	0.025
ko04145	Phagosome	4	0	41	0.003	0.033

18. GO enrichment analysis of DEGs

Table S8. GO enrichment results

Category	GO. ID	GO Term	Up num.	Down num.	Total num.	*P*-value	FDR
OA_L vs Control							
BP	GO:1901071	glucosamine-containing compound metabolic process	13	1	47	6.00E-18	1.03E-14
BP	GO:0006030	chitin metabolic process	12	1	42	5.40E-17	4.63E-14
MF	GO:0008061	chitin binding	12	1	36	1.50E-16	8.58E-14
BP	GO:0006040	amino sugar metabolic process	13	1	60	2.70E-16	1.16E-13
BP	GO:0006022	aminoglycan metabolic process	13	1	96	2.80E-13	9.61E-11
BP	GO:0006032	chitin catabolic process	8	0	22	1.50E-11	4.29E-09
BP	GO:1901072	glucosamine-containing compound catabolic process	8	0	23	2.30E-11	5.64E-09
BP	GO:0046348	amino sugar catabolic process	8	0	24	3.40E-11	7.29E-09
MF	GO:0004568	chitinase activity	8	0	22	1.10E-10	2.10E-08
BP	GO:0006026	aminoglycan catabolic process	9	0	49	6.90E-10	1.18E-07
MF	GO:0004099	chitin deacetylase activity	4	0	4	2.10E-08	3.28E-06
MF	GO:0016798	hydrolase activity, acting on glycosyl bonds	14	0	188	7.10E-08	1.02E-05
MF	GO:0004553	hydrolase activity, hydrolyzing O-glycosyl compounds	12	0	140	1.40E-07	1.85E-05
BP	GO:1901136	carbohydrate derivative catabolic process	9	0	103	5.50E-07	6.74E-05
BP	GO:1901135	carbohydrate derivative metabolic process	23	5	1072	6.50E-07	7.44E-05
MF	GO:0008233	peptidase activity	24	1	740	3.40E-06	3.65E-04
BP	GO:0005975	carbohydrate metabolic process	17	0	548	1.60E-05	1.62E-03

MF	GO:0008236	serine-type peptidase activity	10	0	165	3.40E-05	3.07E-03
MF	GO:0017171	serine hydrolase activity	10	0	165	3.40E-05	3.07E-03
MF	GO:0016811	hydrolase activity, acting on carbon-nitrogen (but not peptide) bonds, in linear amides	6	0	55	5.20E-05	4.46E-03
MF	GO:0016810	hydrolase activity, acting on carbon-nitrogen (but not peptide) bonds	8	0	113	7.00E-05	5.72E-03
MF	GO:0070011	peptidase activity, acting on L-amino acid peptides	19	0	592	1.10E-04	8.58E-03
MF	GO:0008422	beta-glucosidase activity	3	0	10	2.00E-04	1.49E-02
BP	GO:0045907	positive regulation of vasoconstriction	0	3	15	3.50E-04	2.50E-02
MF	GO:0004181	metallocarboxypeptidase activity	3	0	14	5.80E-04	3.98E-02
MF	GO:0019213	deacetylase activity	4	0	33	6.50E-04	4.29E-02
OA_H vs Control							
MF	GO:0042302	structural constituent of cuticle	12	0	26	4.40E-13	7.47E-10
BP	GO:1901071	glucosamine-containing compound metabolic process	11	1	47	2.50E-10	2.12E-07
BP	GO:0006030	chitin metabolic process	10	1	42	1.10E-09	6.22E-07
BP	GO:0006040	amino sugar metabolic process	11	1	60	5.20E-09	2.21E-06
MF	GO:0008061	chitin binding	9	1	36	1.40E-08	4.75E-06
CC	GO:0005833	hemoglobin complex	9	0	37	6.30E-08	1.78E-05
BP	GO:0015671	oxygen transport	9	0	38	9.40E-08	2.28E-05
BP	GO:0015669	gas transport	9	0	39	1.20E-07	2.55E-05
BP	GO:0006022	aminoglycan metabolic process	12	1	96	1.60E-07	3.02E-05
CC	GO:0016459	myosin complex	10	0	57	3.20E-07	5.43E-05

MF	GO:0004099	chitin deacetylase activity	4	0	4	4.10E-07	6.33E-05
MF	GO:0019825	oxygen binding	9	0	43	1.10E-06	1.56E-04
BP	GO:0007602	phototransduction	5	1	18	1.50E-06	1.96E-04
BP	GO:0009583	detection of light stimulus	5	1	19	2.20E-06	2.67E-04
MF	GO:0005506	iron ion binding	13	2	140	2.80E-06	3.17E-04
BP	GO:0006032	chitin catabolic process	6	0	22	5.70E-06	6.03E-04
MF	GO:0043565	sequence-specific DNA binding	5	19	338	6.20E-06	6.03E-04
MF	GO:0016798	hydrolase activity, acting on glycosyl bonds	16	1	188	6.40E-06	6.03E-04
BP	GO:1901072	glucosamine-containing compound catabolic process	6	0	23	7.60E-06	6.79E-04
BP	GO:0006026	aminoglycan catabolic process	8	0	49	9.80E-06	7.71E-04
BP	GO:0005975	carbohydrate metabolic process	28	1	548	9.80E-06	7.71E-04
BP	GO:0046348	amino sugar catabolic process	6	0	24	1.00E-05	7.71E-04
MF	GO:0004568	chitinase activity	6	0	22	1.40E-05	1.03E-03
MF	GO:0004930	G-protein coupled receptor activity	5	5	73	1.50E-05	1.06E-03
MF	GO:0020037	heme binding	13	1	142	1.60E-05	1.09E-03
MF	GO:0009881	photoreceptor activity	4	1	14	1.70E-05	1.11E-03
MF	GO:0046906	tetrapyrrole binding	13	1	152	3.40E-05	2.14E-03
BP	GO:0009581	detection of external stimulus	5	1	32	5.80E-05	3.39E-03
BP	GO:0009582	detection of abiotic stimulus	5	1	32	5.80E-05	3.39E-03
MF	GO:0004553	hydrolase activity, hydrolyzing O-glycosyl compounds	13	0	140	6.00E-05	3.39E-03
MF	GO:0016811	hydrolase activity, acting on carbon-nitrogen (but not peptide) bonds, in linear amides	8	0	55	7.00E-05	3.83E-03
BP	GO:0018298	protein-chromophore linkage	3	3	35	9.80E-05	5.20E-03

BP	GO:0007186	G-protein coupled receptor signaling pathway	7	7	203	1.50E-04	7.71E-03
BP	GO:1901135	carbohydrate derivative metabolic process	37	4	1072	3.00E-04	1.50E-02
MF	GO:0004181	metallocarboxypeptidase activity	4	0	14	3.40E-04	1.65E-02
BP	GO:1901136	carbohydrate derivative catabolic process	9	0	103	4.20E-04	1.98E-02
MF	GO:0008020	G-protein coupled photoreceptor activity	2	1	7	5.30E-04	2.43E-02
MF	GO:0008745	N-acetylmuramoyl-L-alanine amidase activity	2	0	2	6.50E-04	2.90E-02
MF	GO:0003700	DNA binding transcription factor activity	5	14	329	8.00E-04	3.48E-02
PL vs Control							
MF	GO:0003735	structural constituent of ribosome	64	0	994	1.70E-17	3.31E-14
CC	GO:0005840	ribosome	69	0	1128	4.70E-16	4.58E-13
CC	GO:0030529	intracellular ribonucleoprotein complex	90	0	1798	1.10E-15	5.35E-13
CC	GO:1990904	ribonucleoprotein complex	90	0	1798	1.10E-15	5.35E-13
MF	GO:0005198	structural molecule activity	69	0	1363	1.50E-13	5.84E-11
CC	GO:0044445	cytosolic part	43	0	662	7.00E-11	2.27E-08
CC	GO:0044391	ribosomal subunit	42	0	666	3.00E-10	8.34E-08
BP	GO:0006412	translation	74	0	1786	1.60E-09	3.89E-07
BP	GO:0043043	peptide biosynthetic process	74	0	1797	2.10E-09	4.53E-07
CC	GO:0022626	cytosolic ribosome	34	0	506	3.80E-09	7.40E-07
BP	GO:0043604	amide biosynthetic process	74	0	1837	5.60E-09	9.91E-07
BP	GO:0006518	peptide metabolic process	75	0	1918	1.60E-08	2.60E-06
CC	GO:0032991	macromolecular complex	138	0	4419	3.30E-08	4.94E-06
BP	GO:0043603	cellular amide metabolic process	76	0	2025	7.10E-08	9.87E-06

CC	GO:0015934	large ribosomal subunit	25	0	369	4.40E-07	5.70E-05
CC	GO:0022625	cytosolic large ribosomal subunit	21	0	306	3.10E-06	3.77E-04
BP	GO:0018298	protein-chromophore linkage	7	0	35	6.10E-06	6.99E-04
CC	GO:0000502	proteasome complex	15	0	182	9.80E-06	1.00E-03
CC	GO:1905369	endopeptidase complex	15	0	182	9.80E-06	1.00E-03
CC	GO:1905368	peptidase complex	15	0	187	1.40E-05	1.33E-03
BP	GO:0044267	cellular protein metabolic process	114	0	3934	1.50E-05	1.33E-03
CC	GO:0044424	intracellular part	213	0	8565	1.50E-05	1.33E-03
BP	GO:1901566	organonitrogen compound biosynthetic process	83	0	2652	2.90E-05	2.46E-03
CC	GO:0005622	intracellular	219	0	8995	5.20E-05	4.11E-03
BP	GO:0019538	protein metabolic process	122	0	4397	5.30E-05	4.11E-03
CC	GO:0043228	non-membrane-bounded organelle	90	0	2878	5.70E-05	4.11E-03
CC	GO:0043232	intracellular non-membrane-bounded organelle	90	0	2878	5.70E-05	4.11E-03
CC	GO:0015935	small ribosomal subunit	17	0	298	2.70E-04	1.88E-02
CC	GO:0022627	cytosolic small ribosomal subunit	13	0	195	3.30E-04	2.22E-02
MF	GO:0008910	kanamycin kinase activity	2	0	2	3.90E-04	2.53E-02
CC	GO:0005737	cytoplasm	167	0	6503	4.40E-04	2.76E-02
BP	GO:0000387	spliceosomal snRNP assembly	5	0	33	5.40E-04	3.29E-02
CC	GO:0005681	spliceosomal complex	14	0	233	5.60E-04	3.30E-02
CC	GO:0034715	pICln-Sm protein complex	3	0	9	7.70E-04	4.41E-02
BP	GO:0042274	ribosomal small subunit biogenesis	10	0	145	8.60E-04	4.78E-02

19. Disrupted amino acid metabolism

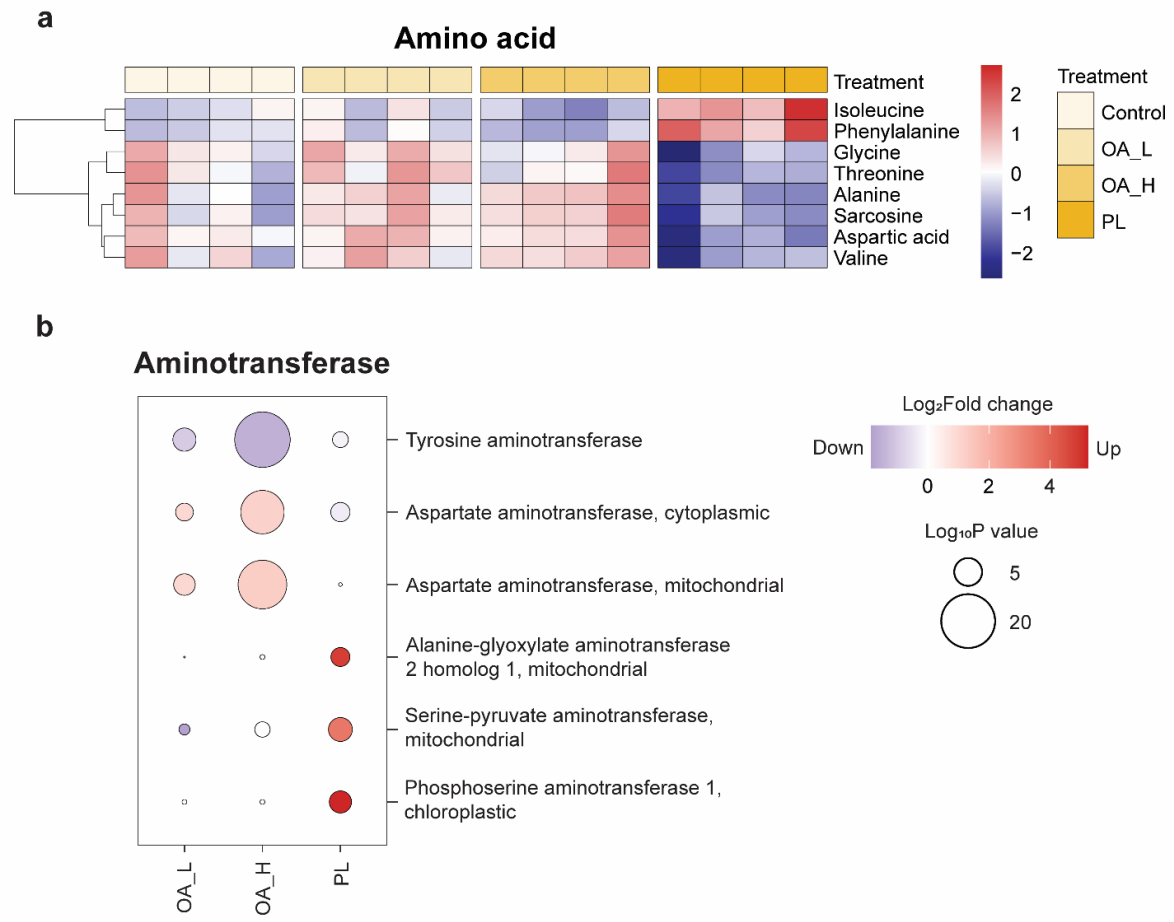

Figure S11. Disrupted amino acid metabolism (a) and aminotransferase expression (b) in adult *A. salina* after exposure to OA or *P. lima*. Metabolomics data were log-transfromed and Z-score scaled before heatmap analysis.

20. Degradation of choline containing phospholipids

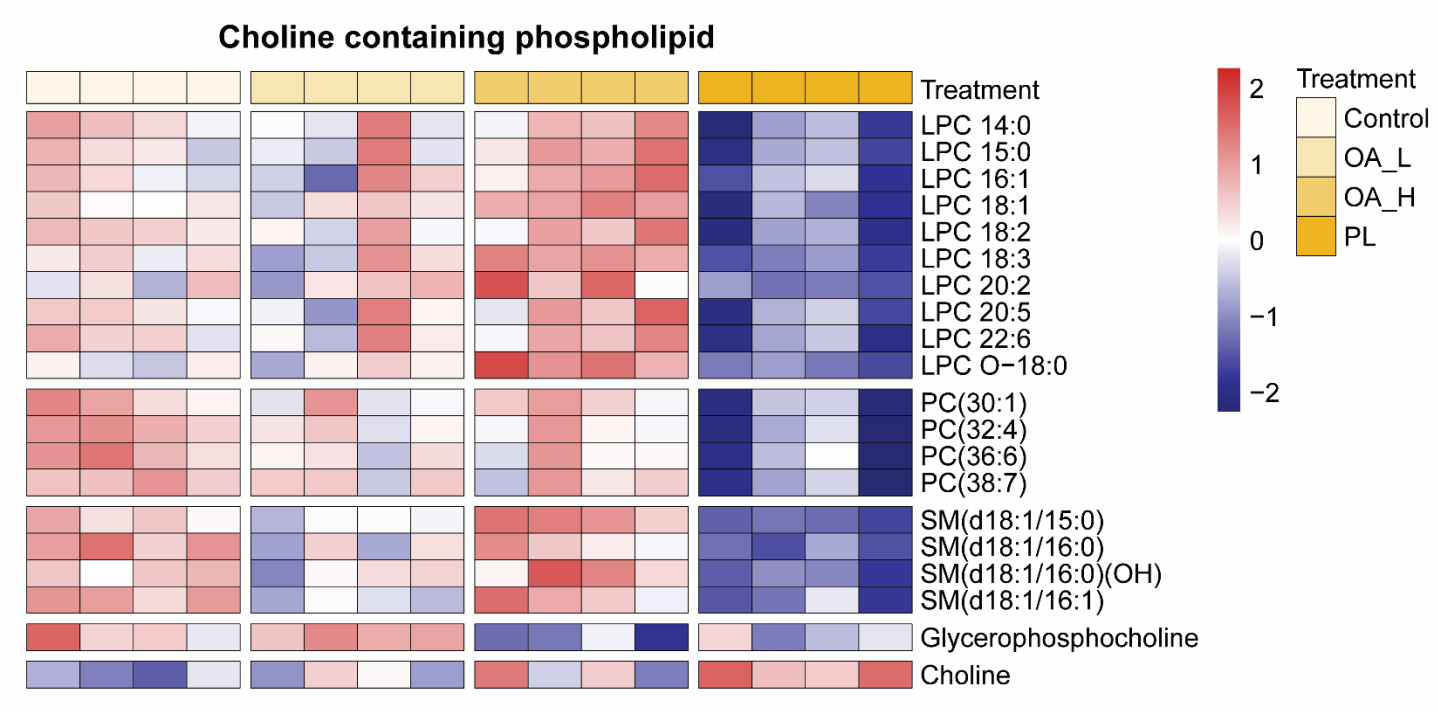

Figure S12. Degradation of choline containing phospholipid in adult *A. salina* by *P. lima* exposure. Heatmap was produced by R package "pheatmap". Data were log-transfromed and Z-score scaled. LPC: lysophosphatidylcholine; LPC O: ether-linked lysophosphatidylcholine; PC: Phosphatidylcholine; SM: sphingomyelin.

21. DEGs involved in proteasomal clearance of damaged proteins, ribosomal protein synthesis and energy metabolism

Table S9. Annotation of DEGs that are involved in proteasomal clearance of damaged proteins, ribosomal protein synthesis and energy metabolism

Gene symbol	Length	Annotation	E-value	Identity
Heat shcok proteins				
Hsp60	1898	heat shock protein 60 [*Brachionus calyciflorus*]	0	59.93%
Hsp70	2113	heat shock cognate 70 protein, partial [*Sesamia inferens*]	0	74.68%
Hsp90	1201	heat shock protein 90 [*Macrobrachium rosenbergii*]	3.36E-57	62.67%
Proteasome				
Pbb2	1073	proteasome subunit beta type-7-B [*Capitella teleta*]	1.10E-109	62.88%
Ppd1	948	proteasome subunit beta 2 [*Xenopus laevis*]	1.47E-59	48.97%
Rpn8b	1616	26S proteasome non-ATPase regulatory subunit 7 [*Sinocyclocheilus anshuiensis*]	1.27E-99	56.99%
Pad1	976	proteasome subunit alpha type-7 [*Sinocyclocheilus grahami*]	8.49E-106	68.02%
Rpn11	1086	26S proteasome non-ATPase regulatory subunit-like protein [*Sarcoptes scabiei*]	4.91E-160	71.06%
Pbe2	1035	proteasome subunit beta type-5-like [*Hydra vulgaris*]	5.03E-105	64.81%
Spliceosome				
Snrpb	1093	small nuclear ribonucleoprotein-associated protein B [*Saccoglossus kowalevskii*]	2.59E-30	56.52%
Snu13	587	NHP2-like protein 1 [*Apteryx australis mantelli*]	3.78E-50	75.36%
Eif4a3a	1283	eukaryotic initiation factor 4A-III [*Lingula anatina*]	0	79.9%

At2g23930	1019	small nuclear ribonucleoprotein G-like [*Acropora digitifera*]	2.88E-25	67.11%
Smd3a	839	small nuclear ribonucleoprotein Sm D3 [*Exaiptasia pallida]*	7.99E-39	56.25%
Snrpe	509	probable small nuclear ribonucleoprotein E [*Nasonia vitripennis*]	1.25E-38	70.93%
Ribosome				
Rps5	1138	40S ribosomal protein S5 [*Falco peregrinus*]	2.69E-115	79.1%
Rps15	960	40S ribosomal protein S15-like [*Saccoglossus kowalevskii*]	3.44E-44	79.31%
Rpl27	618	60S ribosomal protein L27-like [*Hydra vulgaris*]	1.98E-43	56.62%
Rpl18b	762	60S ribosomal protein L18-like [*Lingula anatina*]	6.38E-90	71.96%
Rpl10a	1091	60S ribosomal protein L10a [*Drosophila grimshawi*]	1.41E-90	69.12%
Rpl37a	531	probable 60S ribosomal protein L37-A [*Anopheles gambiae str. PEST*]	1.20E-39	75.28%
Rpl29	355	60S ribosomal protein L29 [*Oryzias latipes*]	6.27E-22	83.02%
Rps20	658	ribosomal protein S20 [*Azumapecten farreri*]	6.73E-64	89.72%
Fatty acid oxidation				
Lacs7	2141	long chain acyl-CoA synthetase 7, peroxisomal [*Nematostella vectensis*]	1.02E-177	43.39%
Lacs3	1382	long chain acyl-CoA synthetase 3 [*Oryzias latipes*]	1.05E-70	47.27%
Lacs5	1241	long chain acyl-CoA synthetase 5 [*Branchiostoma floridae*]	5.96E-62	36.05%
Acx3	2126	acyl-coenzyme A oxidase 3, peroxisomal [*Lottia gigantea*]	1.09E-115	36.76%
Oxidative phosphorylation				
Sdha1	2018	succinate dehydrogenase [ubiquinone] flavoprotein subunit [*Sparus aurata*]	0	70.57%
Vha-e1	887	V-type proton ATPase subunit E1 [*Lottia gigantea*]	4.72E-42	39.57%

Vha-b1	1150	V-type proton ATPase subunit B [*Hydra vulgaris*]	0	83.48%

307

References

1. Conesa, A.; Götz, S.; García-Gómez, J. M.; Terol, J.; Talón, M.; Robles, M., Blast2GO: A universal tool for annotation, visualization and analysis in functional genomics research. *Bioinformatics* **2005,** *21*, (18), 3674-3676.

2. Li, B.; Dewey, C. N., RSEM: Accurate Transcript quantification from RNA-Seq data with or without a reference genome. *BMC Bioinformatics* **2011,** *12*, (1), 323.

3. Livak, K. J.; Schmittgen, T. D., Analysis of relative gene expression data using real-time quantitative PCR and the $2^{-\Delta\Delta CT}$ Method. *Methods* **2001**, *25*, (4), 402-408.

4. Gou, N.; Gu, A. Z. A new transcriptional effect level index (TELI) for toxicogenomics-based toxicity assessment. *Environmental Science & Technology* **2011,** *45*, (12), 5410-5417.

5. Chen, W. -H.; Ge, X.; Wang, W.; Yu, J.; Hu, S., A gene catalogue for post-diapause development of an anhydrobiotic arthropod *Artemia franciscana*. *BMC Genomics* **2009,** *10*, (1), 52.